$NiO-NiFe_2O_4$/MWCNT based Electrocatalyst for Electrochemical Water splitting

By

Rida Noor

School of Chemical and Materials Engineering

National University of Sciences and Technology

2020

$NiO\text{-}NiFe_2O_4$/MWCNTs based Electrocatalyst for Electrochemical Water splitting

Name: Rida Noor

Registration No: 00000172527

This thesis is submitted as a partial fulfilment of the requirement for the degree of

MS in Nano sciences and Engineering

Supervisor: Dr. Muhammad Shahid

School of Chemical and Materials Engineering (SCME)

National University of Sciences and Technology (NUST)

H-12 Islamabad, Pakistan

June 2020

Certificate of Plagiarism

It is certified that PhD/M.Phil /MS Thesis Titled **"NiO-$NiFe_2O_4$/MWCNT based Electrocatalyst for Electrochemical Water Splitting"** by Regn No 00000172527 Rida Noor has been examined by us. We undertake the follows:

a. Thesis has significant new work / knowledge as compared already published or are under consideration to be published elsewhere. No sentence, equation, diagram , table, paragraph or section has been copied verbatim from previous work unless it is placed under quotation marks and duly referenced.
b. The work presented is original and own work of the author (i.e. there is no plagiarism). No idea, processes, results or words of others have been presented as author own work.
c. There is no fabrication of data or results which have been compiled/ analyzed.
d. There is no falsification by manipulating research materials, equipment, processes, changing, omitting result data or result such that the research is not accurately represented in the research record.
e. The thesis has been checked using TURNITN (copy of originally report attached) and found within limits as per HEC plagiarism policy and instructions issued from time to time.

MS Thesis Supervisor
(Dr Muhammad Shahid)
_____ May 2020

Dedication

I dedicate my thesis to my Parents who have always supported and helped me in every best possible way and have always been by my side.

“And make yourself submissively gentle to them (parents) with compassion, and say: O my Lord! Have compassion on them, as they brought me up (when I was) little”. [Al-Isra 17:24).

Acknowledgements

“Truly my prayer and my service of sacrifice, my life and my death, are (all) for ALLAH, the Rabb of worlds”.

I am privileged to express appreciation and gratitude to my research supervisor Dr. Muhammad shahid and my committee members Dr. Zakir Hussain and Dr. Iftikhar Hussain Gul for their constant support, advice, valuable comments, constant persuasion and efficient supervision at every stage of research work. Without their support, this could not have been possible.

I acknowledge my thesis to all my teachers from grade one, who have made me what I am today.

I acknowledge my thesis to all my friends, seniors and colleagues especially Sarosh shamsi, Arman Liaqat, Dooa Arif, Misbah Azad, saira Qayyum and Momena Khan for their support and motivation throughout.

I acknowledge Principal SCME, all faculty members, lab engineers, lab technical staff and non-teaching staff.

Finally, I would like to express my gratitude to all the individuals who have rendered valuable assistance to my study.

Abstract

As with drastically increasing energy demands, environmental concerns and scarcity of conventional fossil fuels, there is high need to look for some efficient enough renewable ways for the production of energy which neither are limited by their scarcity nor environmental and global climate change concerns due to the emission of carbon dioxide unlike conventional fossil fuel resources. Hydrogen due to its light weight, high energy density, storage capabilities and environmental friendliness is considered a quite popular fuel.

The aim of this study was to produce efficient electrocatalyst for water splitting application. Iron doped Nickel oxide nanoparticles were fabricated recognizing excellent oxygen evolution activity of NiO and conductivity increase with Fe incorporation due to its more electropositivity. Electrocatalysts were synthesized with and without surfactant (Tween 85) and both sample types were calcinated at 600^{o}C, 700^{o}C and 800^{o}C. The synthesized nanoparticles were then deposited on GC (glassy Carbon) electrode to check their activity toward water splitting. Samples synthesized in the presence of Tween turned out to be more efficient due to their smaller particle size and porous structure and hence higher activity. Whereas, samples with 700^{o}C outperformed 600^{o}C and 800^{o}C due to formation of NiO-$NiFe_2O_4$ hybrid phase at 700^{o}C temperature. In attempt to futher increase the efficiency and to investigate the effect of MWCNTs incorporation, their nanocomposites with 5%, 10%, 15% and 20% were fabricated with functionalized MWCNTs. Incorporation exhibited significant improvement in activity for 5% and 10 % but at further increase it showed reduction due to filling of pores and reduced percentage of active material (Fe doped NiO). NiO-$NiFe_2O_4$/ f-MWCNTs composite (10 weight%, prepared in the presence of surfactant and calcinated at 700^{o}C) outperformed all the other synthesized electrocatalysts in this study with 35mA/cm^2 of current density at 1.8V.

Table of Contents

List of Figures

List of Tables

Chapter 1

Introduction

1.1 Motivation

Energy since always has played an essential role in the economy of any nation and since its need always has been increasing, this issue is always a major concern. Though our major energy needs are met by fossil fuels but the increasing demands and increasing environmental concern demands to look for some other renewable and clean energy resources.

1.1.1 Energy demands

As the robust energy demands are believed to reach roughly double by 2050 and triple comparing to the present demands by 2100. Therefore, there is high need to look for some other efficient enough renewable ways for the production of energy which neither are limited by their scarcity nor environmental and global climate change concerns due to the emission of carbon dioxide unlike conventional fossil fuel resources. With consistent increase in populations and technological development, energy demands, fuel prices and scarcity is believed continue to increase. Even with rise of 2% per year, energy demands are believed to probably double and triple by the year 2037 and 2057 respectively.

Some of the considered renewable ways which have neither scarcity nor environmental issues are via wind, solar energy, biomass, hydro and tides. All the above mentioned sources have their own pros and cons. Wind and solar energies are quite popular ways but their major limitation is their variability due to the seasons, weather conditions and the day night variations. Though these variations can be handled but these require high cost and capital resources which are still long term issues for developing countries. Similarly, for hydropower dam's erection is a challenge which again requires high costs.

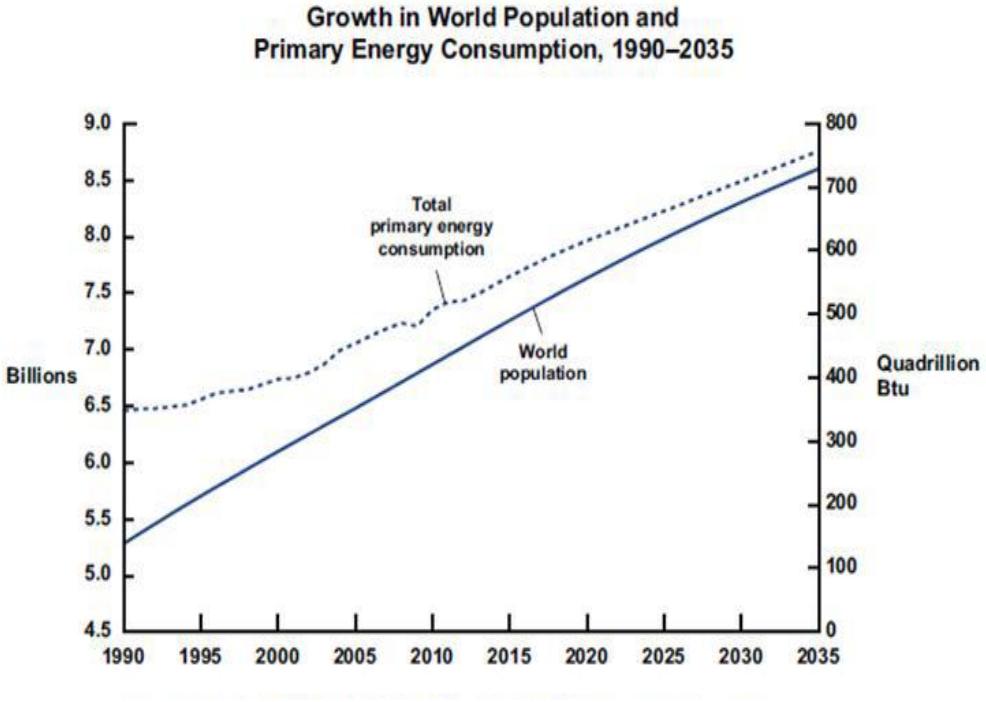

Figure 0-1 Showing increasing energy consumption trend[1]

Fuel production through water splitting is considered as one of the best way to meet such concerns. As water is not only abundant but is a clean source of hydrogen emission. Hydrogen due to its light weight, high energy density, storage capabilities and environmental friendliness is considered a quite popular fuel.

1.1.2 Why hydrogen

Fading conventional fuel resources, renewability, nontoxicity and climate change considerations make hydrogen a potential candidate as a fuel. Since oil crises in late 20th century, economic growth has been effected due to increasing energy demands by industries and transport sector. Energy costs per unit growth in demand should be reduced in order to increase economic growth. Therefore, to meet increasing needs of energy in the modern era is of great interest. One of the other major issues of this modern age of technology is increasing pollution causing climate change and greenhouse effect. Hydrogen fuel are zero emission fuel and hence the best consideration to overcome this issue.

1.1.3 Future Scope

Significance and need of establishment of clean and renewable hydrogen fuel is accepted worldwide but only practical effects towards implementation of this technology can determine its potential.

Countries highly developed in technology, majorly including Japan and USA have realized the scope of hydrogen as future energy source. USA government had entitled 10 years' program for the implementation of hydrogen fuel setup and invested $1.7billion and due to which by 2030 750,000 new jobs are also expected. Japan also had invested $240m in 2002 for the development of hydrogen fuel infrastructure. By the end of 2018 availability of 265,000 domestic fuel cells with 5KW of capacity, 100 fuel cell forklifts for industrial use and 2,800 FCVs (fuel cell vehicles) demonstrates Japan's commitment towards hydrogen fuel technology. Japan aims 40,000 and 800,000 FCVs by2020 and 2030 respectively. And in order to achieve this target the Ministerial council on Renewable Energy introduced a strategy to reduce hydrogen fuel prices up to one fifth of its current prices by 2050. Reduction in hydrogen fuel prices competitively conventional fossil fuel resources will pave way for FCVs target. Japan is also planning to use FCVs at Olympics 2020 to showcase hydrogen fuel and fuel cell potential. Napal and many other countries are also making considerable efforts towards this technology.[2]

1.2 Challenges

Despite the development of science and technology there are still some challenges and difficulties for the implication of hydrogen fuel due to the following reasons.

1.2.1 Storage issues

Gravimetrically hydrogen is 14 times lighter than air. Therefore, for the transportation of it requires either heavy and costly containers or its conversion in liquid form. But still its compression requires intensive energy which also is an expensive way and strong and expensive materials for containers are required for its safe transport and to overcome cracking through hydrogen embrittlement. However, cryogenic or compressed hydrogen is the best considered way for its transportation and carbon-fiber storage tanks are

recently being used due to their high strength and light weight which makes these superior than steel tanks.

1.2.2 Cost effects

Till now cost for fuel production through electrolysis is 3-6 times more than from natural gas. Though in case of electrolysis costs for labor, extraction and refining is not required but electricity cost is the major hurdle as for the production of 1 kilogram, 35KWh of electricity is required. This shows that hydrogen fuel cost is linearly linked with electricity costs.[3]

Some other considerable challenges for this technology is the need of establishment of infrastructure and safety considerations. Hydrogen being flammable and unique properties requires special safety considerations.

1.3 History of water splitting

The phenomenon of water splitting was discovered back in 1789 b y A.P Van Troostwijk and J.R Deiman while performing an experiment with two gold wires dipped inside water. When electricity was passed through the system, gas evolution occurred. Later in 1800 Anthony Carisle and William Nicholson identified these gases as oxygen and hydrogen. Afterwards 1869 when Zenobe Gramme invented Gramme machine (electrical generator), water electrolysis got economical and industrial significance. The next 5 decades from 1920 onwards proved to be golden era for development of industrial hydrogen production technology through water splitting. By 1939, first plant for hydrogen production was established with the capacity of 10,000Nm3H2h-1. A lot of efforts were made for the development of this technology and various kinds of electrolysis systems got established e.g PEM (polymer exchange membrane) electrolyzer.

Hydrogen production through water electrolysis was considered quite popular in fertilizer industry for ammonia manufacturing, till the first half of the 20th century which was then replaced by hydrogen production through hydrocarbons due to their low cost and mass production. However by 1970, oil crises, increasing concerns of fossil fuel

scarcity and global warming again inclined the interest in fuel production through water splitting.[4][5]

1.4 Mechanism of water splitting

Water splitting is an endothermic reaction and hence requires energy to initiate the reaction. This energy is usually in the form of electrical energy and hence is known as electrochemical water splitting.

General equation for water splitting in alkaline electrolyte is:

$$2H_2O \rightarrow 2H_2 + O_2$$

Hydrogen gas is evolved at cathode while oxygen gas at cathode. The following reactions occur at anode and cathode:

Cathode (reduction):

$$2H_2O + 2e^- \rightarrow H_2 + 2OH^-$$

Anode (oxidation):

Step 1: $4OH^- \rightarrow OH^* + 3OH^- + e^-$

Step 2: $OH^* + 3OH^- + e^- \rightarrow O^* + H_2O + 2OH^- + 2e^-$

Step 3: $O^* + H_2O + 2OH^- + 2e^- \rightarrow HOO^* + H_2O + OH^- + 3e^-$

Step 4: $HOO^* + H_2O + OH^- + 3e^- \rightarrow O_2 + 2H_20 + 4e^-$

Unlike hydrogen evolution oxygen production by direct recombination is not possible. As OER occurs in multiple steps requiring electrons in each step hence they have got a wide activation potential barrier. Therefore, in water splitting reaction though hydrogen evolution is easy but oxygen evolution requires manipulation with anode catalyst to obtain relatively lower activation potential. [6]

Hydrogen and oxygen evolution occur at cathode and anode respectively. Both cathodic and anodic reactions are equally responsible for rate of reaction and hence efficiency.

However, hydrogen evolution reaction is comparatively easy while oxygen evolution is a little challenge.

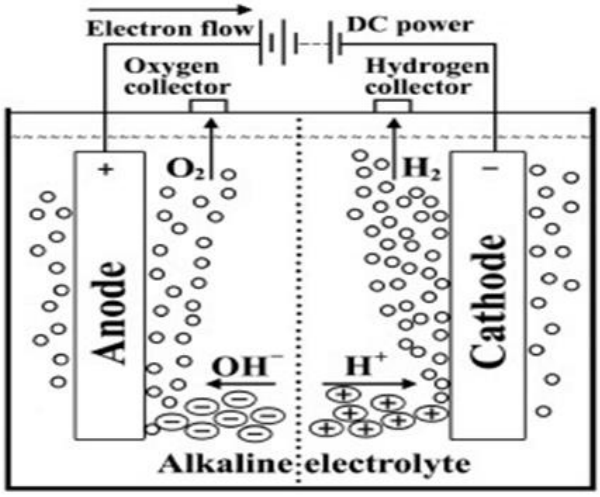

Figure 0-2 Basic mechanism of water splitting cell[4]

This slow OER (oxygen evolution rate) is due to high activation energy for the transfer of four electrons and hence search of an efficient OER catalyst is required. A lot of research on fuel production through water splitting has been conducted since last few decades but still they are far from sufficient and there is still wide room for research. Therefore, this research is intended to contribute in finding the best possible cheap, abundant and highly efficient catalyst material with high turnover frequency catalysts.

1.5 Applications of hydrogen:

The miscellaneous applications of hydrogen are:

- As a rocket fuel due to its high energy density and light weight.
- As an automobile fuel instead of conventional petroleum, due to its zero-emission.
- In petroleum refinery industry for the removal of sulfur and conversion of long chained molecules of hydrocarbons into shorter.
- In hydrogen welding (atomic form) where it not only generates temperature of up to 4000°C but prevents from reacting with other elements.

- In Ultraviolet lamps its deuterium isotope is used to generate ultraviolet light which in laboratories is then used for spectroscopic analysis.
- As a reducing agent in various reactions.
- In chemical analysis via atomic absorption spectroscopy and gas chromatography.
- In generation of electricity through nuclear reactors heavy water is usually used as coolant to slow down neutrons and that heavy water can be made by deuterium (isotope of hydrogen).
- In balloons due to its light weight and low cost but being explosive enough is being replaced by helium.
- In fabrication of mass destructive bombs as weapon.
- Hydrogen's combination with oxygen forms hydrogen peroxide which is used in hospitals and clinics as sterilizing agent.
- For fabrication of vegetable oil by hydrogenation of unsaturated fatty acid molecules.

U.S has established 60 outdoor hydrogen fuel stations for fuel cell vehicles. Hydrogen fuel cell stations are aimed to be used as uninterrupted energy supply to hospitals, telecommunication and data centers etc.

As oxygen is also a useful product in water electrolysis hence some applications are mentioned below:

- For emergency breathing purposes in hospitals, rockets and submarines etc.
- Liquid oxygen is carried in rockets as an oxidizer as is essential for burning.
- In water treatment plants it is used to help benevolent bacteria to breakdown dangerous compounds for waste water treatment.
- In some bars flavored oxygen is used as mood booster and stress releaser though its use is not considered save.
- Due to its low density it is used as a coolant in various appliances, computers and rockets etc.

- In industries oxygen is used in steel mills, for welding and fabrication of acetylene and methanol etc.

1.6 Types of Electrolyzers

In pursuit of designing best possible water splitting system, various electrolytic systems have been fabricated. Some of the main types of electrolyzers are PEM (proton exchange membrane) electrolyzers, Solid Oxide electrolyzers and AES (Alkaline Electrolytic systems).

1.6.1 Proton Exchange Membrane Electrolyzer (PEM)

Proton Exchange membrane electrolytic cells as its name indicates are based upon solid polymer electrolytes that facilitates the proton transport between electrodes (cathode and Anode) during electrolysis. The desired characteristics of a membrane include good mechanical, chemical and oxidative stability, high durability and excellent proton conductivity. Usually perfluorosulfonic acid based polymers such as Felmions, Nafions, Aciplexs and Fumapems are used for membrane fabrication to obtain these characteristics. The optimum membrane thickness is however an important consideration that enables high proton conductivity without much loses and hence lower over potentials. PEMs are however a bit expensive due to costly polymers.

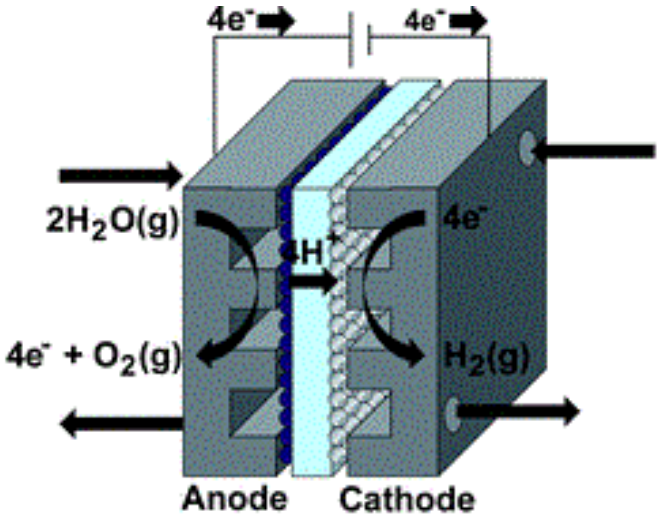

Figure 0-3 Proton exchange membrane electrolyzer [6]

1.6.2 Solid Oxide Electrolyzer (SOE)

Solid Oxide Electrolyzers are high temerature electrolyzers that operate at around 600-900^{o}C, use steam instead of liquid electrolyte and generally require relatively lower overpotentials. Oxygen anions are transported from cathode to anode through solid electrolyte that is usually made of yttrium zirconium oxides. They are relatively less costly which makes them attractive if heat source is available.

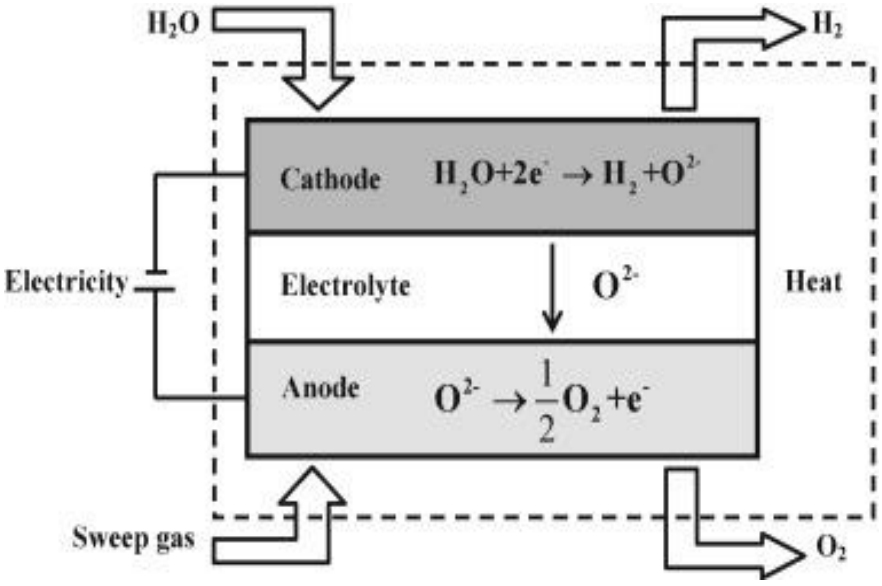

Figure 0-4 Solid Oxide electrolytic cell [7]

1.6.3 Alkaline Electrolyzers (AES)

These are the most commercialized electrolyzers among all other types for large scale production of hydrogen. This type of electrolyzer is based upon alkaline electrolytes, usually KOH and NaOH. Metal oxides with optimum porosity and hence surface area are used as electrodes for high Hydrogen evolution. Usually Ru and Ir oxides are considered as electrode materials however due to their scarcity and high costs, doped nickel oxides are their effective replacement. [8]

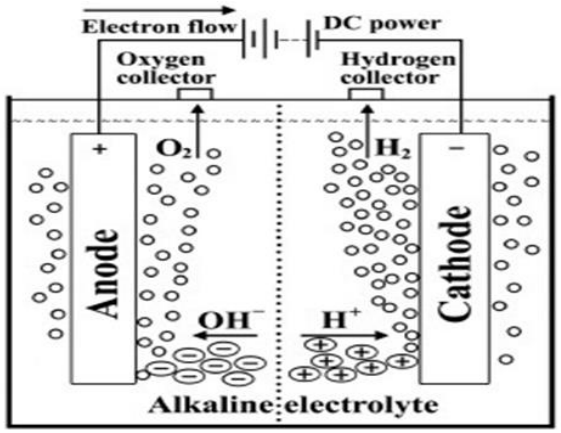

Figure 0-5 Alkaline Water Electrolyzer [4]

1.7 Water Electrolysis Mechanism

Water electrolysis is the process of separating oxygen and hydrogen molecules of water of water molecules by passing a direct current through it. And therefore, electrolyzer is an electrochemical device as indicated by its name, which converts electrical energy into chemical energy. And that chemical energy is then stored in the form of fuel which can further be used to perform useful works by converting into other required form of energy. At the surface of electrodes, ions either gain or lose electrons generating oxygen and hydrogen gas. Electrons are gained at cathode polarizing it negatively, where hence reduction occurs and hydrogen is produced. Whereas, electrons are lost at anode polarizing it positively, where hence oxidation occurs and oxygen is produced.

While talking about its thermodynamics, electrolysis is a non-spontaneous and endothermic process as it requires overpotential for the process to initiate. The minimum voltage required for an electrolysis process to take place is termed as V_{rev} (reversible voltage), while for water electrolysis minimum voltage required is termed as V_{tp} (thermal potential voltage). For a real system V_{tp} should always be greater than V_{rev}. The reason for this is electrical and thermal losses as the system is not adiabatic and hence radiation and convection may cause losses. The energy required to drive an electrolysis process is also affected by temperature and pressure. According to literature less energy is required for this process at higher temperatures.[9]

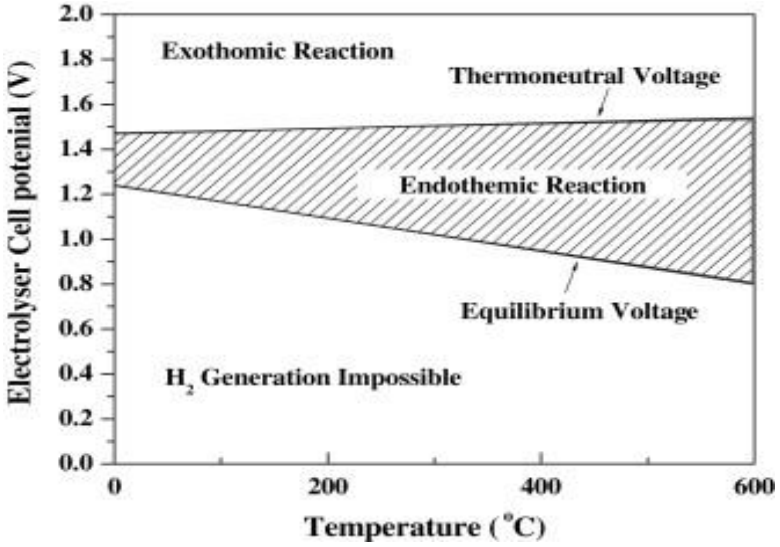

Figure 0-6 Effect of temperature change on electrolyzer potential.[10]

The above mentioned diagram illustrates the idea of temperature effecting electrolyzer potential. The graph is divided into three regions. As discussed previously, the minimum theoretic voltage required for the water electrolysis to take place is equilibrium potential or V_{rev} whereas thermos-neutral voltage or V_{tp} (Thermal potential voltage) is the actual potential required for the process to take place. And as due electrical and thermal thermos-neutral value should always be greater than equilibrium reaction for a real system to proceed a reaction. Below equilibrium voltage electrolysis is not possible and hence no hydrogen gas is produced. Above this potential electrolysis take place. In the shaded region reaction is endothermic after a certain voltage limit if the voltage is further increased, the reaction becomes exothermic. As the temperature is increased value of equilibrium voltage decreases. However, thermos-neutral voltage has comparatively a very little influence of temperature.

The relationship between the potential and the current generated is usually illustrated by tafel plots. Electrochemists usually use this graph to find the resistivity and hence information about corrosion such as corrosion rate and passivity etc. As electrolysis involves oxygen and hydrogen evolution the given tafel plot indicates both half reactions involved in water electrolysis.

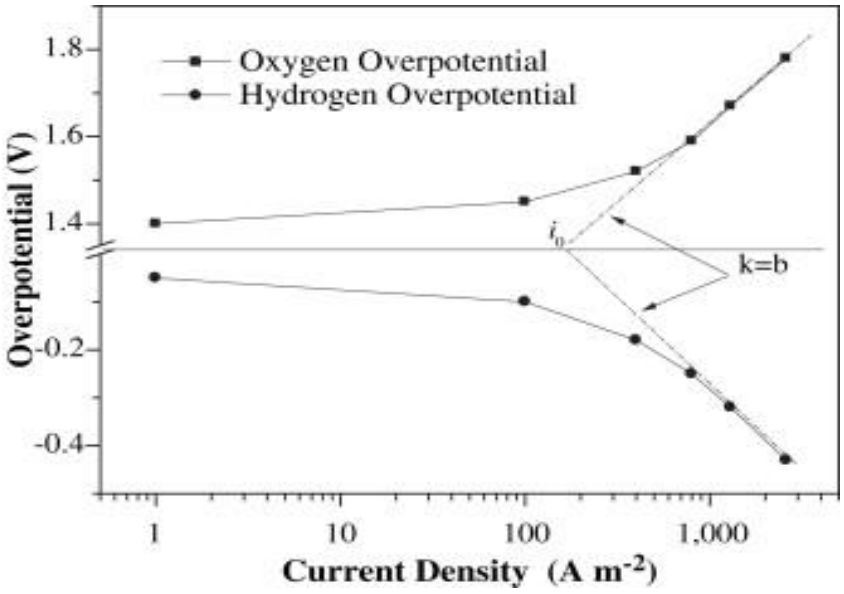

Figure 0-7 Tafel plot for water electrolysis [9]

The upper or positive region of a tafel plot indicates anodic reaction where oxygen evolution is occurring. The lower negative region of a tafel plot indicates cathodic reaction where hydrogen evolution is occurring. k in the graph indicates the slop. The slops from the anodic and cathodic reactions help in finding the value of equilibrium current density and equilibrium potential of a system. [8]

For ideal water electrolysis system minimum potentials to derive anodic and cathodic reactions are 1.23V and 0V respectively. But due to some losses minimum 1.4V is required for a practical anodic reaction. Lower the slop and higher the current density, higher will be the activity of an electrode.[11]

To understand the thermodynamics of water electrolysis a bit more, pourbaix diagram is intended to be discussed in this paragraph. Pourbaix diagram illustrates the effect of pH on the potential of a system. The below mentioned Pourbaix diagram is for a water electrolysis system. It consists of three regions. Upper and lower regions in the diagram indicate hydrogen and oxygen evolution regions while middle region indicates thermodynamic stability of water. The diagram indicated that the change in PH affects the value of potentials required for the redox reactions. Nernst equation is used to find the redox potential of a cell under nonstandard conditions e.g pH change etc.

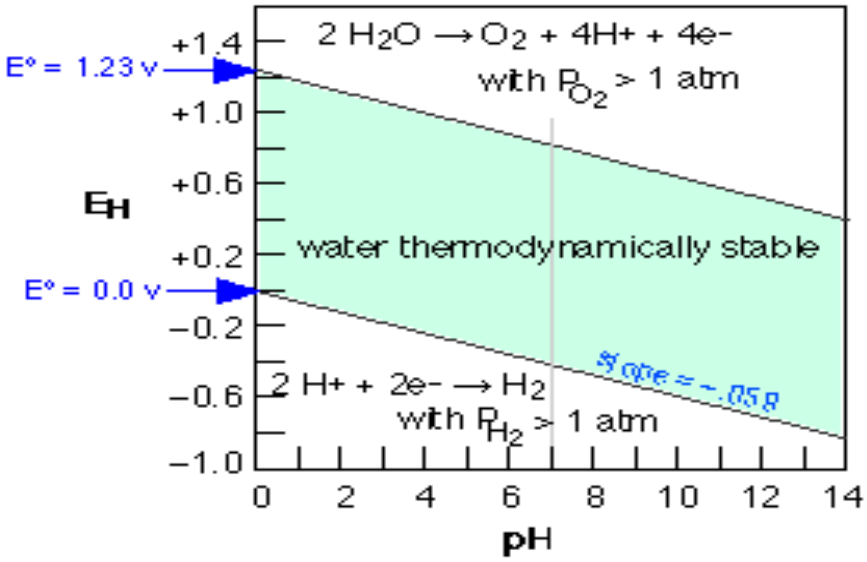

Figure 0-8 Pourbaix diagram of water electrolysis [12]

Nernst equation:

$$E = E° - \frac{RT}{nF} \ln \frac{[red]}{[oxi]}$$

Where

E= redox potential E^o = standard electrode potential under standard conditions

R = general gas constant T = temperature

F = Faraday constant n= no of electrons taking part in redox reaction

[red] and [oxi] stands for molar concentrations of oxidation and reducing agents respectively.

By putting constants values we get Nernst equation as

$$E = E° - \frac{0.0592}{n} \ln \frac{[red]}{[oxi]}$$

For water electrolysis system Nernst equation in terms of pH can be written as

$$E = E° - \frac{0.0592}{n} \times pH$$

For hydrogen reduction at cathode, putting the standard electrode potential E^o = 0V and n=1 we get Nernst equation as E = -0.0592 ×pH V at standard temperature and pressure. Which indicates that, pH increase decreases the potential. Similarly, for oxygen evolution at anode, standard electrode potential is 1.23V which forms Nernst equation as, E= 1.23 -0.0592 ×pH V. which also indicates the decrease in potential with increasing potential. [13]

1.8 Materials

Though for water electrolysis minimum voltage limit is 1.23V at 0pH, standard pressure and room temperature but still the real system requires higher potential, which is called overpotential. However greater value of overpotential means lower efficiency. Hence, reduction of overpotential has always been a great interest. [14] In efforts to reduce overpotential and to increase the efficiency, a lot of catalysts with single and multi-metal phases, metal oxides, amorphous oxides, spinal and layered hydroxides structures have been designed. Oxygen evolution reaction OER as is little harder than hydrogen evolution reaction HER as four electrons are involved in this reaction and therefore, high overpotential is required to overcome this activation barrier. Hence OER catalysts are comparatively of high interest. Water oxidation catalysts (WOCs) with higher efficiency, more stability, corrosion resistance, lower costs and abundance are intended.[15]

Metal oxides are considered as one of the most important candidates of WOCs family due to their higher electrical conductivity, atomic diffusivity, oxygen ion mobility and catalytic activity. Their high catalytic activity is attributed to the presence of different kinds of defects including vacant lattice sides, electron- whole pairs, interstitials sites, dislocations and impurity etc.[15][16]

1.8.1 Rare Metals and their oxides

Ir, Ru, IrO_2 and RuO_2 are considered as the best known catalysts for both acidic and basic media. However, their industrial application for water electrolysis is limited due to their scarcity and high costs.[17] $IrO_x/SrIrO_3$, Cu_2O, Cu_2O/ITO, Ir_xO/ATO and TiO_2/

CuO also have been studied widely.[18] Electrochemically synthesized RuO_2 is reported to show better performance comparing to chemically synthesized RuO_2 but its stability is lower therefore IrO_2 is considered as a better option.[19] The reason for their priority is believed to be the stability of the intermediates that are formed during oxygen evolution reaction.[20]

Some metallic catalysts form stable oxide layers and show good electrolytic activities but not all metallic catalysts are suitable. For example Ru when is used in metallic form rather than its oxide form, it shows very good OER but oxide layer formed on its surface is not stable and eventually starts dissolving during reaction.[21]

1.8.2 Earth abundant metals and their oxides

Although rare earth metals Ru, Ir and their oxides show excellent performance towards OER but still due to their high costs, research on highly efficient earth abundant materials is of great interest. Some of the efficient abundant elements, their oxides and mixtures are intended to be discussed here.

1.8.2.1 Cobalt oxide

Co_3O_4 is considered to show good OER efficiency. Their good performance is attributed to Co_4p cation forming Oxos, which can interact well with water molecules. Co_4p and Co_3p cations create active sites which facilitate OER. Tuning of Co_3O_4 structure by doping or creating vacancies has shown improvement in its performance.

Some other factors which play important role in OER efficiency are particles size and morphology. Reduced particle size causes increase in surface area leading to the availability of more active sites whereas; morphology contributes to the diffusivity of molecules. Therefore, optimization of particle size is important as reduction of particle size changes both the surface energy and morphology. Doping is considered to improve the performance of electro-catalyst by introducing non uniformity of charge distribution and reducing crystallite size. With smaller crystallite sizes charge transfer occurs easily and OER is facilitated.[22]

1.8.2.2 Manganese oxide

Manganese due to its poor conductivity is not considered an excellent choice for OER electro-catalyst. However, addition of other conductive metal catalysts has shown the improvement in its performance significantly. Addition of even less than 5% of Au nanoparticles has shown 6 times more OER performance by formation of Mn_3p active sites.[23]

α-MnO_2 comparing to β-MnO_2 is a better candidate for an efficient electro-catalyst due to spacious channeling of its structure which provide good opportunity for diffusion of charged species unlike later structure which has narrower channeling and hence can't contribute well in diffusion.[24]

In the case of Mn_3O_4 , simultaneous presence of Mn_2p and Mn_3p enhances its performance both as OER (oxygen evolution reaction) and ORR (oxygen reduction reaction) electrocatalyst.[25]

1.8.2.3 Copper oxide

Cu is not only cheaper than Ni and Co but also has distinct coordination chemistry but still its oxides are not considered much efficient as electro-catalysts. But its incorporation and mixtures with other electro catalyst can significantly enhance their efficiency. Therefore cu complexes can be used to tune copper oxides structure which then show good electro-catalytic performance.[26]

1.8.3 Mixed metal oxides

Mixture of two or more transition metal and their oxides in optimum amounts can form complex structure which can be used as efficient OER catalysts. Nickel iron oxide mixture for instance shows noticeable efficiency towards OER. Iron is this mixture makes catalyst conductive and also provides active sites for reaction.[27]

$CoFe_2O_3$, $NiCo_2O_4$, $MnCo_2O_4$, $CuCo_2O_4$ and $ZnCoO_4$ are some of the other noticeably good electro-catalysts. The reason of their good performance is attributed to the non-uniform charge distribution which causes the introduction of active sites. But along with the active sites high conductivity is also desired which can be achieved doping with

metals with high conductivity.[28] For instance good performance of NiO with Fe doping is due to conductive nature of Fe which facilitates charge transfer.

1.8.3.1 Perovskite metal oxides

Perovskites have great importance as an OER catalyst especially in fuel cell applications. According to research the perfect kind of perovskites are the one who have e.g close to unity.[21] Catalytic activity of $Ba_{0.5}Sr_{0.5}Co_{0.8}Fe_{0.2}O_2$ is reported to increase during cycling which is quite interesting, because in other cases it usually reduces during cycling. The reason behind that is believed its surface amorphization during cycling process and it is a vital advantage of perovskites.[29]

1.8.4 Metal Hydroxides

As during electrolysis hydroxide layer is formed on the metal oxides therefore, metal oxides and hydroxides are somehow considered similar. Similar to metal oxides, incorporation of more than one transition metals (having different sizes), changes the lattice structure and forms more active sites. For example incorporation of Fe into $Co(OH)_2$ is believed to increase its efficiency around 100 folds.[30]

1.8.4.1 $Co(OH)_2$

Just as cobalt oxides, their hydroxides have also been studies as electro-catalysts but still due to their deprived conductivity they are not considered best candidate. However doping with other conductive species can sufficiently enhance their performance.[31]

In case of electrochemical deposition of $Co(OH)_2$ films, electrode substrate is an important factor for its activity. Comparing to Cu and Pd, Au shows noticeably good activity due to substrate's electro negativity. During cycling, crystallinity of the electrode surface is increased which as discussed earlier effects the electro-catalytic activity and makes it sluggish. Lattice structure is rearranged during cycling of OER and therefore the non-uniformity turns towards uniformity resulting less availability of active sites. All $Co(OH)_2$ films go through this mechanism and therefore their performance with increasing number of cycles decline.[32]

1.8.5 Metal sulfides, phosphides and selenides

Just like metal oxides, metal sulfides, phosphides and selenides have successfully been studied for electro catalytic applications as transition metals are the one who are responsible to provide active sites and not the anions.

1.8.5.1 Nickel sulfides

Nickel sulfides also have been studies widely and are considered good candidates for electrolysis. Their performance is dependent upon their crystal structure and morphology. Ni_3S_2 lattice structure consists of NieNi bonds network which shows good metallic behavior. Therefore, they are considered efficient OER catalysts. However, they are unstable in OER which is a hurdle for its practical applications.[33]

1.8.5.2 Cobalt sulfides and Selenide

Cobalt Sulfides are considered to show good ORR (oxygen reduction reactions) but they show sluggish performance towards OER (oxygen evolution reaction). Therefore, there is high need of reduced OER over-potential for its efficient bi-functional performance. Research depicts that the bi-functional performance of Co_9S_8 can be improved by the incorporation of metal oxides. Incorporation of metal oxides introduces metal- oxygen bonds on cobalt sulfide structure which break Co-O bond and form Co super oxide bond which can participate well in reaction.[21]

CoSe and $CoSe_2$ are two stable cobalt selenides which are known for their good electro catalytic performance both for OER and ORR. However, in bulk form they show poorer performance and needs exfoliation for the availability of active sites.[34]

1.8.5.3 Mixed metal selenides

Just like mixed metal oxides, metal selenides also show improved performance. For instance, $Ni_{0.5}Fe_{0.5}Se_2$ is reported to show far better OER efficiency than $FeSe_2$ and $NiSe_2$. Their improved performance is due to their morphology which provides opportunity for the availability of the active sites.[21]

1.8.5.4 Nickel phosphide

Unlike metal oxides and other materials, nickel phosphides have been the most underrated materials for electro catalytic applications despite of their good catalytic performance. However, since past few years they have attracted researcher's attention. According to research it is even believed that there might be the possibility that Ni_2P can show better performance than nickel oxides and their hydroxides. Yu et al. reported that porous structures of nickel phosphides exhibited highest OER efficiency in acidic media among nickel oxides, hydroxides and phosphides prepared by the same method.[35]

1.8.6 Metal carbides and nitrides

Unlike other metal oxides and sulfides, active sites in carbides and nitrides are not formed by oxygen vacancies or defects but they have ordered lattice structures. For instance, graphene which has a highly ordered 2D hexagonal lattice structure is not efficient for OER as doesn't provide much active sites but in an ordered manner. Research shows that Co_4N can be a potential candidate. Just like metallic Co, this also forms cobalt oxide film during OER.[36]

1.8.7 Active metals

Intrinsic conductivity of active metals (e.g Ni, Fe, Mn, Co etc.) makes them attractive candidates for OER. They usually form oxides layers on their surface during OER mechanism. One of the pitfalls of spontaneous formation of oxide layer on their surface is uncontrolled composition of their lattice structure but still their fresh growth is advantageous for aging issues. Active metals also show poor stability towards corrosion which is a major obstruction in their practical application. However their instability can be tackled by surface treatment but their OER should not be compromised in this approach.[37]

Fig1.9 depicts that overpotential of electro-catalyst significantly is reduced by increasing the number of active metals in an alloy. The reason behind this efficiency is attributed to the non- uniform distribution of charged cations which contribute in generating more active sites.

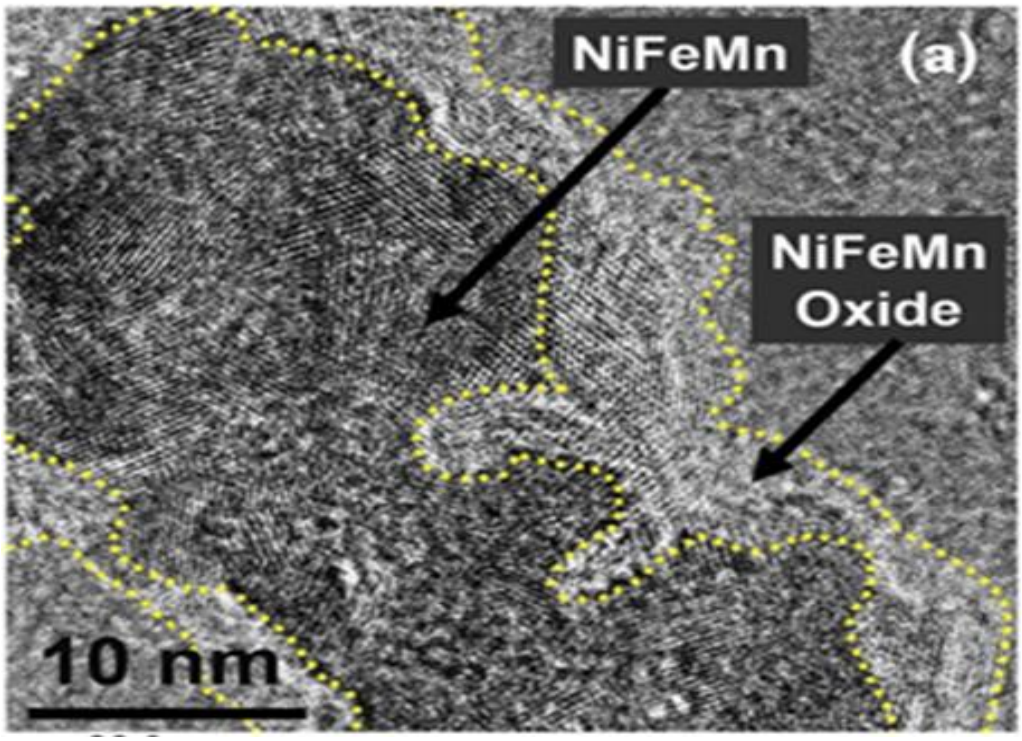

Figure 0-9 HRTEM image of NiFeMn catalyst. Dashed yellow line indicates a few nm thick oxide layer formed on its surface.[38]

1.8.8 Carbon-based electro-catalysts

1.8.8.1 Metal free carbon electrodes

Although due to highly ordered lattice sp_2 hybrid structures, OER overpotentials of carbons are sufficiently high but their low costs, good conductivity and design versatility somehow makes them attractive for electro-catalytic applications. But there is a high need of activation of sites which can participate well in OER and can be generated by manipulating hexagonal sp_2 network. However, dangling bonds at edges are easier to manipulate than sp_2 networks.

Several approaches are there for the manipulation of carbon network for active sites. A few of these include defect engineering, incorporation of elements with different sizes and functionalization with reactive groups. Doping with S, P, N and B is considered the most promising approach for this purpose. N is considered the best dopant among all the aforementioned dopants when chemical activity is concerned.[39]

1.8.8.2 Carbon as a conductive agent

Carbon based nano-materials such as CNTs and graphene have widely been used to form electro-catalytic nano-composites due to their high surface area and conductivity. But these nano-composites require chemical interaction through proper functional groups. CNTs are believed to form shortcuts between electro-catalyst and CNTs.[40]

1.8.9 Why Ni and its incorporation with Fe?

High efficiencies, affordability, stability and environmental concerns are always the crucial criteria while researching on the best possible electro catalyst. Transition metal oxides because of all these qualities have been an attractive candidate for researchers. Their low costs, abundance and high OER activity enables them to stand out for their performance without having to compromise with expenses. However, Ni and Ni alloys among all the other transition metals have been considered the most efficient for electrolysis in alkaline media.[41] Ni as having oxidation state +2 (in NiO) which is compatible to the oxidation state for OER, is an active OER catalyst but has got comparatively poor crystallinity which can be improved by incorporation of conductive metals. Comparing to pure NiO its alloys with Fe, Mo and Co have been proven to be efficient for electrolysis. However, iron is considered the most efficient as far as conductivity is concerned. Interestingly due to the strong affinity between Ni and Fe, Fe is commonly found as impurity with Ni compounds in nature and researchers discovered that iron's impurity enhances the OER activity of the catalyst which diverted researcher's attention towards NiFe compositions.[42] As it is a universally acknowledged fact that smaller particle sizes lead to the greater surface area and hence improved activity but crystallinity and hence conductivity is compromised this way. Therefore, for the optimization of activity and conductivity simultaneously, incorporation of Fe in NiO plays a significant role.[42]

1.9 Objectives

In the light of the motivation and all the aforementioned discussions in this chapter, the main objective of this research work is to contribute in research by fabrication of the efficient OER catalyst (as OER is the major obstacle in water electrolysis process).

The core objectives of this research work are as follows:

- ✓ The synthesis of Iron doped NiO Nanoparticles using co-precipitation method without Surfactant (Tween).
- ✓ The synthesis of Iron doped NiO Nanoparticles using co-precipitation method with Surfactant (Tween).
- ✓ Functionlization of MWCNTs.
- ✓ Fabrication of their composites with functionalized MWCNT.
- ✓ Study of structural and morphological properties by characterizing the synthesized electro-catalyst.
- ✓ Deposition of the synthesized electro-catalyst on GC for the fabrication of anode.
- ✓ Utilization of these fabricated Anodes for the Study of Electrochemical properties of the synthesized electro-catalyst and checking their efficiency towards water splitting application.

Chapter 2

Literature Review

Ksenia Fominykh et al[43] in 2014 for the first time fabricated ultrasmall, dispersible and crystalline NiO NPs (nanoparticles) electrocatalyst via solvothermal process, for water electrolysis applications. Nanoparticles of around 3.3nm with excellent dispersibility and very narrow size distribution were fabricated which outperformed RuO showing 0.29s-1 turnover frequency at 0.3V overpotential. Highly dispersible and crystalline NiO NPs allows its deposition on temperature sensitive substrates as for crystallinity high temperatures are not required enabling it attractive candidates not only for water electrolysis but also for solar cells applications.

Ksenia Fominykh et al.[44] in 2015 synthesized $Fe_xNi_{1-x}O$ nanoparticles in tert-butanol using solvo-thermal process. He kept doping concentration of Fe up to 20% and observed decrease in particle size with increasing concentration of iron. 10% Fe doped particles showed superior OER efficiency and turn over frequency even higher than IrO catalyst in basic media. He attributed the smaller particle size by increasing Fe content to the presence of Fe on the surface of NiO which prevents its further growth during synthesis. Synthesized particles with high crystallinity and large surface area proved to be efficient OER electro-catalyst due to good conductivity and high activity respectively.

Xien Liu et al.[45] in August, 2015 published a facile synthesis method for the composites of nitrogen doped rGO (reduced garaphene oxides) with Ni and Co oxides as multifunctional electro-catalysts. These composites were prepared by the process of pyrolysis. Both the fabricated multifunctional electro-catlysts of Ni-NiO/rGO and Co-CoO/rGO proved to be excellent electro-catalysts towards not only OER (oxygen evolution reaction) but also towards HER (hydrogen evolution reaction). These composites showed $10mAcm^{-2}$ of current density for 0.24V of over-potential for OER. These electro-catalysts are claimed to be superior to expensive IrO electro-catalysts. Their composites with graphene are highly effective due to their magnificent electrical

conductivity and surface area leading to the availability of more active sites and charge transfer capabilities.

Xing Zhang et al[46] in December 2015 also published facile method for the fabrication of bi-functional composites of Fe_xNi_{1-x} /NC. Similar to aforementioned research, these composites were also prepared via pyrolysis approach using metal salts and urea and Iron doping concentration depicted to affect the performance of electro-catalyst. Fe_xNi_{1-x}/NC electro-catalyst loaded on porous Ni foam is claimed to show excellent OER, HER and good stability. The composite was reported to show $10mACm^{-2}$ of current density for 1.58V of over-potential.

Lena Trotochaud et al[47] studies effect of intentional and unintentional electrochemical incorporation of Fe in Nickel hydroxide and oxy-hydroxide films. Effects on structures, electronic properties and OER performance were examined. Fe inclusion showed almost 30 fold improved activity in basic media. Though increase in number of cycles effect the order or disorder of structure however its effect on OER performance is negligible comparing to the effect due to inclusion of iron impurities from electrolyte. The improved performance is attributed to the charge transfer capabilities of Fe.

Rui Xiang a et al[48] in 2018 fabricated economical and ecofriendly bi-functional $FeNi(OH)_x$/Ni electro-catalyst by corrosion of Nickel substrate in the presence of $Fe(NO_3)_3$. Stable and uniform $FeNi(OH)_x$/Ni nanosheets were grown on Nickel foam substrate without the need of any binder and showed efficiency even higher than RuO in alkaline media. These nano-sheets on porous nickel foam substrate not only provide abundant active sites for OER but also good bubble diffusion. Coupling of corroded substrate and hydrolysis of Fe^{+3} ions proved to be an effective way for efficient bi-functional electro-catalyst for water splitting.

Geng Wua et al.[49] in 2017 reported the synthesis of iron doped nickel oxide nanotubes mustered by around 10 atomic layer thin nano-sheets for water electrolysis application. These electro-catalysts showed not only excellent performance with $10mAcm^{-2}$ of current density at 0.31V but also showed excellent stability. Fe

incorporation is believed to provide abundance of Ni^{+3}/Ni^{+4} and Ni vacancies due to its higher electronegativity resultantly increasing its efficiency. As smaller particle size is necessary for higher surface area and hence activity but it also causes aggregation during OER process reducing its stability. However, these hierarchical structures containing Ni^{+3} active sites, and unique geometry are proved to be attractive candidates for such issues.

Ruoyu Zhang et al[50] in 2016 reported the fabrication of an electro-catalyst by ALD (atomic layer deposition) of Ni/NiO on a carbon fiber paper followed by annealing. The fabricated catalyst showed $10mAcm^{-1}$ of current density at over-potential of 0.189V and 0.257V for HER and OER respectively with good stability in basic media, hence is considered a good candidate for anode and cathode in two electrode system.

Mary W. Louie et al[51] in 2013 prepared Ni, Fe and Fe-Ni based electro-catalytic films via electro-deposition over gold electrodes and studied their relative efficiencies towards water electrolysis. Ni-Fe films with 40% of iron content showed 3 and 2 folds higher OER efficiency comparing to pure Fe films and pure Ni based films respectively. Over-potentials of 230mV, 400mV and 500mV with current density of $10mAcm^{-2}$ are reported for Ni-Fe, Fe and Ni based films. Increasing efficiency with increase of iron content is attributed to the Fe as being more electronegative Fe reduces oxidation state of Ni.

C.R.P. Patel et al[52] in 2018 reported the fabrication of GC (graphene Carbon) nano-composites as catalysts anode for water electrolysis applications in basic media. Various compositions of GC were prepared which showed improved activity comparing to pristine graphite while GC73 (70% graphene and 30% Carbon) exhibited most favorable performance with 487I/hm2 of hydrogen production and prevention from graphene agglomeration. Enhanced performance was attributed to the presence of more active sites within composites resulting lower activation energy.

Ming Gong et al[53] in 2014 reported the synthesis of Ni/NiO nano-composite with CNTs via hydrolysis. Ni/CNT, NiO/CNT and CNT alone showed inferior HER (hydrogen evolution reaction) performance comparing to NiO/Ni-CNT composite.

Outperformance of NiO/Ni-CNT composite is credited to its higher surface area and collaboration of NiO and Ni.

Mikaela Gorlin et al[54] in 2016 reported the fabrication of Ni-Fe oxy-hyroxide electro-catalyst and studied the OER dynamics and charge transfer mechanism using DEMS (operando differential electrochemical mass spectroscopy) and XAS (x-ray absorption spectroscopy). The results reveal the constant +3 oxidation state of Fe and increase in oxidation state of 75% of Ni from +2 to +3 while the rest 25% show +4 during OER. Ni-Fe(OOH) with various Fe percentages were investigated ranging from 0-100 % of iron content and in this study at 50% Fe catalyst showed highest activity. The investigations suggest that depending upon Fe:Ni stoichiometry, no separate metallic Ni, Fe or their oxides are formed but catalyst consists a mixed bimetallic phase. Fe maintains its oxidation state being independent of Fe:Ni stoichiometry but it being more electronegative than Ni changes its oxidation state. Ni in as prepared Ni(OH)2 contains +2 oxidation state but under OER catalyst with certain Fe content it changes its oxidation state which facilitates OER activity.

Yong Xu et al[55] in 2019 reported the synthesis of bi-functional $NiFe_2O_4$ anchored CNTs based catalyst by mean of super critical CO_2. Fabricated composites of very small $NiFe_2O_4$ NPs of range 5-10nm uniformly anchored over CNTs, showed efficient OER and HER efficiencies of 150mV and 240mV respectively with $10mAcm^{-2}$ of current densities in basic media. Conductivity, high surface area and chemical stability are the properties which make CNTs an attractive candidate for electro-catalytic composite but still its hydrophobicity is a great challenge towards controlling the uniform growth of nanoparticles over CNTs. So, instead of organic compounds which tend to agglomerate and collapse CNTs, in this work super critical CO_2 is used considering its high penetration, strong solvent capabilities and low viscosity which could make possible the good dispersion of particles over vertically aligned CNTs.

Alaa Y. Faid et al[41] in 2019 reported the synthesis of Ni, NiCo and NiFe based oxides via co-precipitation method for electro-catalytic applications. 33 mole% of Ni composition exhibited highest activity due to the smallest crystallite size and hence largest surface area among all aforementioned compositions. Beside the compositional

differences the effects of binder were also considered for study. Nafion and Fumion FAA-3 were used for comparison. Nafion showed better results toward HER in comparison to Fumion FAA-3.

Abdul Qayoom Mugheri et al[56][15] in 2019 reported the fabrication of Co_3O_4/ NiO composite as an electro-catalyst for hydrogen production through water electrolysis. Being inexpensive, abundant, simple structured materials and beneficial interface chemistry, its composites are a good choice comparing to Pt and RuO_2. This composite has proved to be the efficient bi-functional catalyst for OER and HER in alkaline media, with reduced impedance and enhanced activity compared to single NiO or Co_3O_4. This composite is reported to be promising candidate for water splitting applications with Tafel slopes for OER and HER with the values of $61mVdec^{-1}$ and $101mVdec^{-1}$ respectively.

Shide Wu a et al[57] in 2019 reported the derivation of Fluorine doped $NiCo_2O_4$ metal organic frame works from Ni/Co metal organic framework (MOF) via solvothermal process. The proposed Fluorine doped nanostructure is the combination of NiO, CoF_2 and $NiCo_2O_4$ embedded porous carbon matrix ($NiCo_2O_4$/NiO/CoF_2@mC) which contains immense active sites for the catalytic process. Various compositions with and without fluorine doping and also with various calcination temperatures were studied for comparison. Fluorine doped structure at 700^oC calcination temperature ($NiCo_2O_4$/NiO/CoF_2@mC700) showed the best results for both HER and OER in comparison to without fluorine doping and other fluorine doped structures with 600, 800 and 900^oC. $NiCo_2O_4$/NiO/CoF_2@mC700 exhibited the $10mAcm^{-2}$ of the current density with -45mV and 1.47V of over-potentials for HER and OER respectively. While the small Tafel slopes of $78mVdec^{-1}$ for OER and $29mVdec^{-1}$ for HER were obtained. These structures are reported to show not only good activity due to synergistic effect and homogenous distribution of nanoparticles over the carbon matrix but also show excellent stability and durability.

Hongtao Yu et al[58] in 2019 reported the fabrication of bi-functional, binder-free and recyclable Ni/NiO nano-dots as an electro-catalyst over Ni foam using electro-deposition technique. NiO/NiND@NF exhibited $10mAcm^{-1}$ of current density over an

over-potential of 1.70V with high stability. The efficiency of the catalyst is attributed to the roughness of its surface and porous structure which enables the exposure of more active site. Large electrode of approximately 70cm^2 was also constructed successfully. Moreover, solubility of the contents in acidic media (0.5M HNO_3) makes it easy to recover the raw material. Reporter also investigated the corrosion behavior of Ni foam in acidic media and mentioned the process for the recovery of the NiO/NiND. No significant corrosion of Ni foam in the aforementioned $Ni(NO_3)_2$ can simply be recovered for further use which is also environmentally friendly.

Aniruddha Mondal et al[59] in 2018 reported the protocol for the synthesis of hollow NiO spheres via spray drying of nickel ammonium carbonate solution. Porous structures with 10-16nm of size and 120m^2/g of surface energy were obtained at calcination of 300^oC. Fabricated NiO hollow spheres exhibited excellent performance with 10$mAcm^{-2}$ of current density at over-potentials of 0.37V and 0.424V for OER and HER respectively in alkaline media. The effective performance of these catalysts is itself due to its hollow sphere which provides large surface area and hence more availability of active sites inside out of the structure, leading to the efficient gas molecule diffusion as well as charge transport.

Lishan Peng et al[60] in 2018 reported the fabrication of Ni foam supported $NiONi_3S_4$ hetero-nanosheets electro-catalyst via in-situ sulfuration. NiO/Ni_3S_4 interfacial structure, nanosheets excellent electronic properties and Ni foam's porous structure contribute to its good performance towards both OER and HER with 20$mAcm^{-2}$ current density at 0.29V and 10$mAcm^{-2}$ of current density at 71mV of Over-potential respectively. Investigation of the efficiencies of different compositions resulted the outperformance of $NiONi_3O_4$ /NF over NiO/NF, Ni_3O_4 and RuO_2. Moreover, small Tafel slopes of 75$mVdec^{-1}$ and 70$mVdec^{-1}$ for OER and HER respectively also exhibited the outperformance of $NiONi_3O_4$/NF over other aforementioned compositions.

Fang Song et al[61] in 2019 published a paper regarding Iron Nickel electro-catalyst in which they claimed the outperformance of the synthesized catalyst over all the other existing reported Iron Nickel oxide catalysts. Characterizations revealed covalently bonded γ-FeOOH and γ-NiOOH nanoclusters. Catalyst was electrochemically deposited

over Ni Foam. For substrate comparison catalysts were also electrodeposited over Au and GC (Glassy Carbon) substrates. Both showed almost similar performances to deposition over Ni Foam.

Chapter 3

Introduction to Characterization Techniques

1.10 Introduction

To thoroughly examine the properties of materials various characterization techniques are used. The concerning characterization techniques of this research work are intended to be discussed in this chapter. Following are the techniques which have been used:

a) X-Ray Diffraction (XRD)

i. Phase formation

ii. Crystallite Size

b) Scanning Electron Microscope (SEM)

i. Surface morphology

ii. Structural observation

c) Fourier Transformed Infrared Spectroscopy (FTIR)

d) Brunauer, Emmett and Teller (BET)

i. Porosity

ii. Surface area

f) Cyclic Voltammetry (CV)

1.11 X-Ray Diffraction (XRD)

X-ray diffraction is a non- destructive characterization which is used to study crystal structures, phase identification, crystal orientations, strain and crystallite size of all kind of materials including solids, powders, fluids and crystals. Back in 1985, W.C. Rontgen discovered it for the first time. Metallurgy, Mineralogy, archeology, metallurgy, geology, biology, forensic sciences and pharmaceutical sciences are some of the various fields where it is widely used.

1.11.1 Working principle of XRD

The basic principle of XRD is the diffraction of x-rays from the crystal planes as both the x-rays wavelength and inter-planar spacing are comparable and hence satisfy the condition for diffraction. The x-rays when interact with the planes, diffract at different angles. These angles are measured, analyzed by the processing unit and then diffraction peaks are obtained on monitor.

The various diffracted rays while interacting with each other either cancel each other's effect or undergo reinforcement depending upon their phase difference and hence undergo destructive and constructive interference respectively. Brags gave us the condition for destructive interference according to which constructive interference occurs only if the path difference is integral multiple of wavelength.[62]

Mathematical statement of Brags law is

$$2d\sin\theta = n\lambda$$

Where,

n= angle of diffraction

λ= wavelength of X-rays

θ= angle of diffraction

d= interplanar spacing

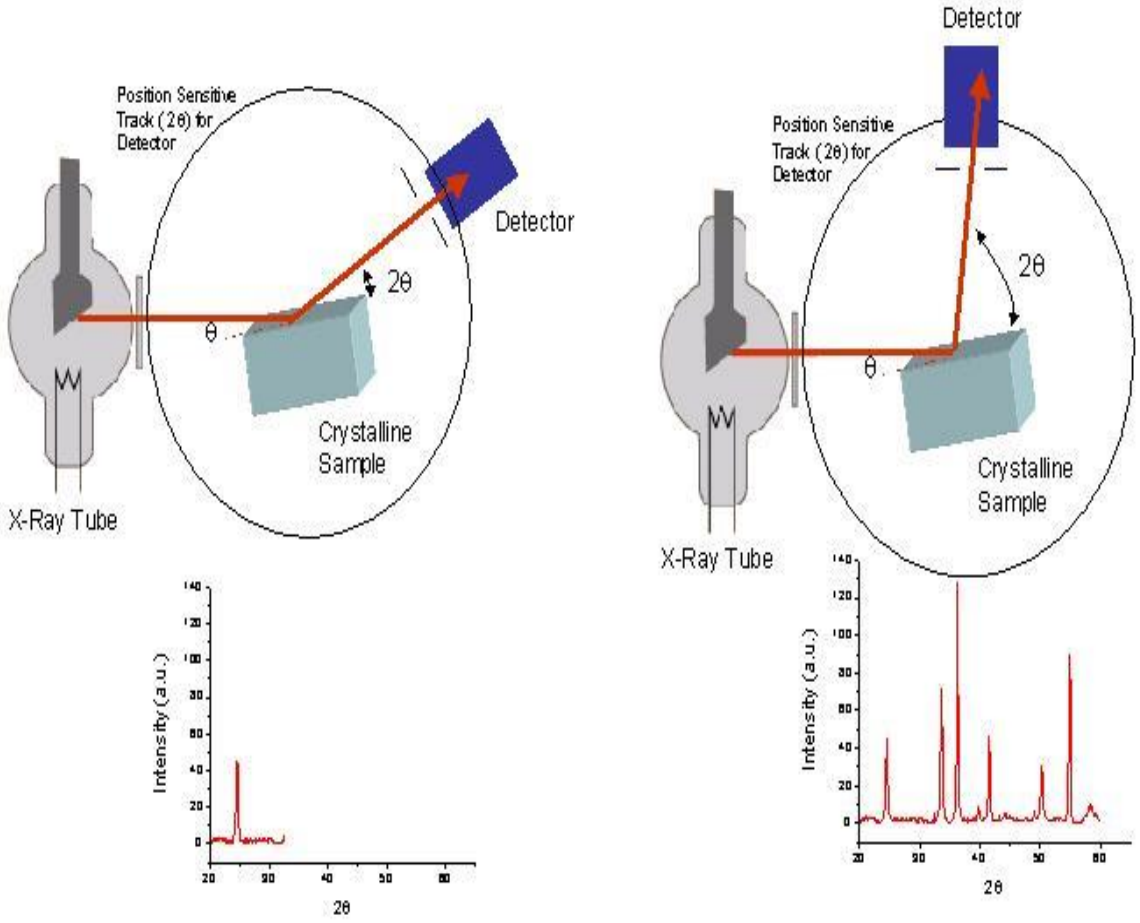

Figure 0-1 Schematics of XRD[63]

1.12 Scanning Electron Microscopy (SEM)

Scanning electron microscopy is a non-destructive imaging technique in which a high energy beam of electrons focused using magnetic lenses is scanned over the sample to obtain image. The signals generated as a result of interaction of electron beam gives information about morphology, topography, crystalline structure and compositional differences. Images from the selected or desired area can be collected using this technique.

Figure 0-2 SEM instrument[64]

1.12.1 Working principle of SEM

High energy electrons while interacting with the sample dissipate their energy in generating different kinds of signals including secondary electrons, backscattered electrons, auger electrons, x-rays, diffracted backscattered electrons and heat. Out of these all signals secondary and backscattered electrons are detected by the SEM detectors to collect information. Detection of morphology and topography is attributed to the secondary electrons whereas backscattered electrons give contrast in composition.

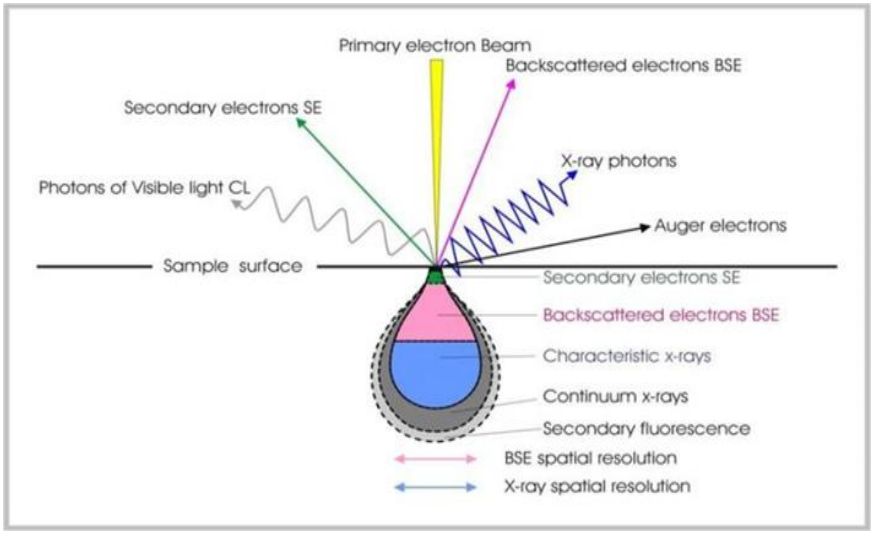

Figure 0-3 Signal generated in SEM[65]

Main components of SEM instrument include electro gun, electron lenses (to focus beam), sample stage, detectors and processing unit (to analyze collected signals). SEM at least contains one detector essentially for secondary electrons but some instruments can have more than one detector depending on their specifications.[66]

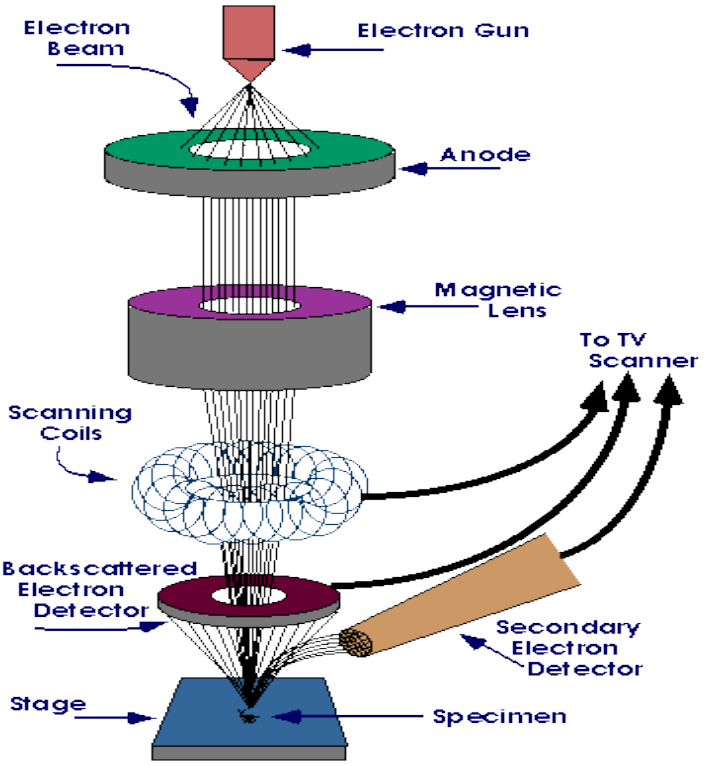

Figure 0-4 Schematics of SEM [67]

1.13 Fourier Transform Infrared Spectroscopy

Fourier transform infrared spectroscopy (FTIR) is an adsorption spectroscopy in which absorption or emission infrared spectrum of material is obtained. Usually it is used to study organic compounds for instance polymers etc. In comparison of dispersive spectrometer, infrared spectroscopy can measure intensities over a wider range of wavelengths. This superiority has created more opportunities for various fields to use this technique especially in biology and biomedical applications.[68]

1.13.1 Working principle of FTIR

FTIR uses an incandescent light source for the emission of radiation in infrared range. This IR beam is incident over a beam splitter which splits it half towards a movable

mirror while the other half towards a fixed mirror. After reflection through both mirrors when beams arrive at the same point they interfere either constructively or destructively depending upon their path difference. This interfered beam is then sent toward the sample placed in its path and then towards detector. This IR radiation causes characteristic vibrations (stretching or bending) in the molecules of sample. The signals are then processed and spectrum is obtained.

1.13.2 Sample preparation for FTIR

1% (w/w) of sample with KBr (potassium bromide) dye is mixed and is compressed in a hydraulic press at pressure of 10,000 psi. The pallet is then scanned at the rate of 4mm/s over 400-4000 cm^{-1} wavelength range.[69]

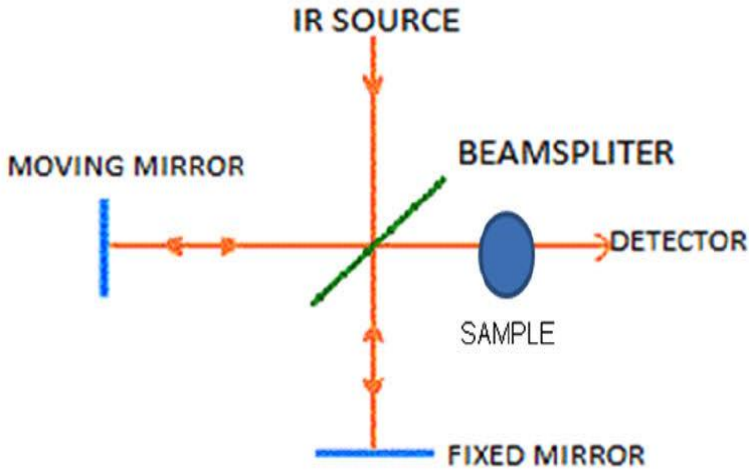

Figure 0-5 Schematics of FTIR spectrometer[70]

1.14 Brunauer, Emmett and Teller (BET)

Porosity and surface area are the properties that play vital role in the activity and performance of a nano-material. Hence, pore size and surface area measurements are sometimes very important while determining the efficiency of a material and there Brunauer, Emmett and Teller (BET) is the most commonly used technique. Commonly BET is the reliable and suitable technique to get pore size and surface area information through Nitrogen sorption for the porous materials within the pore size range of ~20 Å

to ~ 0.15μm. For materials with larger pore sizes mercury porosimetry is used which can determine the pore size of up to ~200μm accurately.

1.14.1 Mechanism

In this technique the material is exposed to the Nitrogen gas at certain conditions and then by estimating the adsorption or desorption, pore size distribution, pore size, pore volume and skeletal density of the material are determined. Knowing the cross-sectional area of the adsorbed nitrogen molecule (16.2 $Å^2$/ molecule) and monolayer capacity, surface area of the material is measured. Porous materials always have greater areas comparing to nonporous materials.

Experiment is performed at relative pressure (p/p_o) of 0.3, where P_o is saturation pressure. At 77K and 30% of nitrogen saturation pressure, the experiment is carried out. During probe gas exposure after the formation of monolayer over the surface of material, capillary condensation starts occurring within the pores of the material. During this whole process, condensation first occurs in smaller pores following the filling of larger pores as the relative pressure is increased.

The following figure depicts an adsorption desorption isotherm of a porous material with respect to changing relative pressure (P/P_o) at 77K. Lower curve and upper curve depict adsorption and desorption respectively. Starting part of the isotherm gives information about the surface area as monolayer is formed initially at lower relative pressures but as the relative pressure is increased pores start to be filled so the latter part of the curve is used to get information about total pore volume. Different types of the porous materials exhibit different types of isotherms. Isotherms with a hysteresis loop are obtained in the case of mesoporous materials while the macro porous materials don’t show hysteresis.

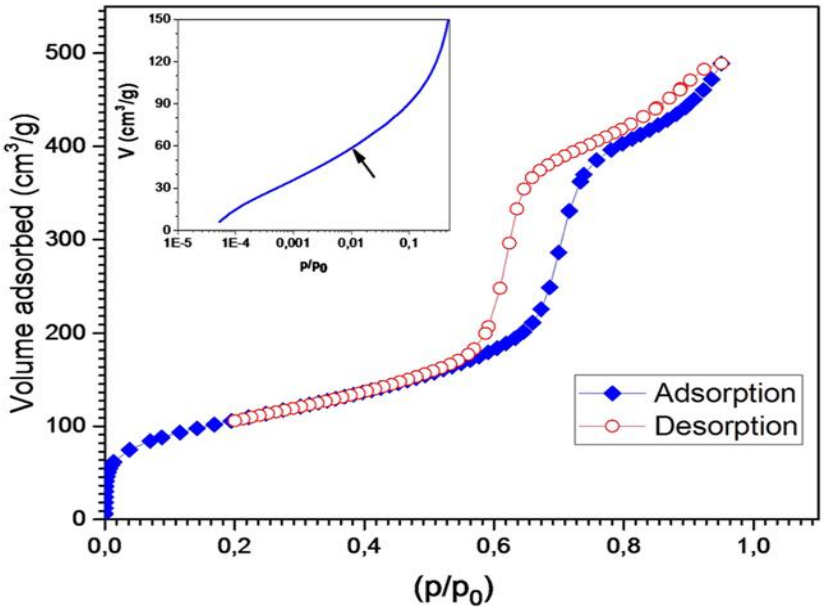

Figure 0-6 sorption isotherm of a porous material[71]

1.14.2 Sample preparation

Sample preparation conditions are crucial aspects to be considered before sorption analysis as for accurate and reliable pore size and surface area measurements, the removal of gasses which may have adsorbed under ambient conditions is very essential. Since under ambient atmosphere significant amount of gas molecules are absorbed which may fill the surface and pores of the materials resulting in the inaccurate results, so heat treatment of the sample at optimum temperature for the removal of these molecules without changing the original sample surface is highly intended. Optimization of the heat treatment temperature and time are essential considerations and require high care for selection as it can highly influence results by increasing and decreasing the pore size. As under mild conditions, the pore blockage may not be removed completely while at high temperature the sample's surface properties might be affected by sintering or decomposition.[72]

1.15 Cyclic Voltammetry (CV)

Cyclic voltammetry is an electrochemical technique in which varying potential is applied across the working electrode to obtain a voltammogram (IV curve), through which developed current is measured. Or in other words it is a technique to measure the

half reaction potential or oxidation/reduction potentials through a complete voltammogram, after providing the sufficient time for the completion of redox cycle. It is a widely used electrochemical technique not only in electrochemistry but also in organic, inorganic and bio chemistry due to its ease of measurement and fast redox behavior study. Concentration of solution can also be found by calibrating current vs concentration graph, as current is proportional to the concentration of the solution.

1.15.1 Mechanism

As indicated by its name the potential of a working electrode which is submerged in a suitable electrolyte, is cycled against a reference electrode to measure current. The applied varying potential across working and reference electrodes can be referred as excitation signal. The excitation signal is usually a triangular waveform consisting two switching potentials.

Potential of the working electrode is changed linearly with respect to time. Cycle starts from the potential at which no redox reaction takes place and then the potential is changed gradually until reduction or oxidation takes place and then linear sweep is reversed. As illustrated in the following figure, in forward scan (a to d) when value of potential is decreased linearly with respect to time until the potential is obtained where oxidation or reduction can now take place, as denoted by the point d which is also known as switching potential. After that the reverse scan starts (d to g) where potential is increased until it is sufficient for the other half reaction to take place and similarly, the cycle can be repeated. During forward scan (a to d) where potential is scanned from higher to lower value, reduction takes place whereas, during reverse scan (d to g) where potential is scanned toward higher potential, oxidation takes place. However, the scan rate for cycle can be varied.

During potential sweep at working electrode current can be measured to obtain voltammogram. Cyclic Voltammogram which is also known as IV curve contains current and voltage along vertical and horizontal axis respectively. In the following figure cyclic voltammogram is shown in which redox reactions are indicated as a result of forward and reverse scans. During forward scan (a to d) when potential is decreased gradually reduction takes place and the resulting current is known as cathodic current.

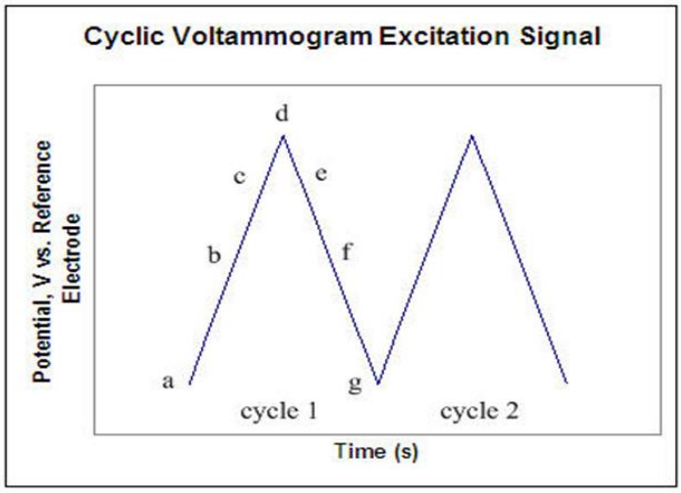

Figure 0-7 Cyclic Voltammogram Excitation Signal [73]

The point c indicates the optimum cathodic potential, where maximum cathodic current is developed. After the switching potential d reverse scan starts where potential is increased and in this region oxidation takes place. Point f indicates the optimum potential for oxidation at which maximum oxidation takes place and the entire electrode surface is oxidized. [74][75]

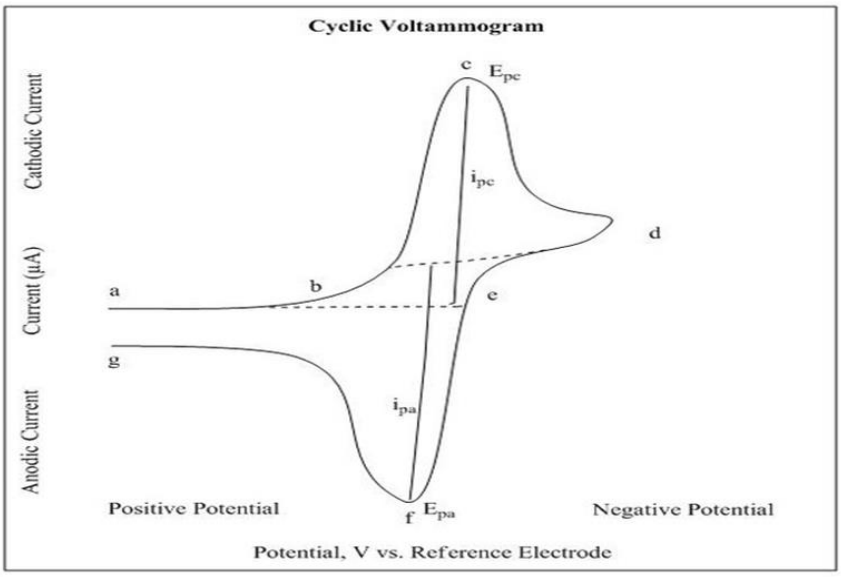

Figure 0-8 Cyclic Voltammogram[73]

CHAPTER 4

Materials and Experimentation:

1.16 Experimentation

1.16.1 Synthesis of $NiFe_2O_4$ Nanoparticles without Tween

Iron doped NiO nanoparticles were synthesized by co-precipitation method. Iron to Nickel ratio was kept as 15:85. Solution of 1M NaOH in 50ml deionized water was prepared by pouring 2mg of NaOH in 50ml of DI water under stirring at temperature of 60°C and was denoted as solution 1. Another 2.5M solution of $Fe(NO_3)_3.9H_2O$ and $Ni(NO_3)_2.6H_2O$ in 20ml of DI water was prepared by adding 3mg and 12.35mg of iron nitrate and nickel nitrate respectively. This solution was denoted as solution 2 and was stirred well enough for 1 hour.

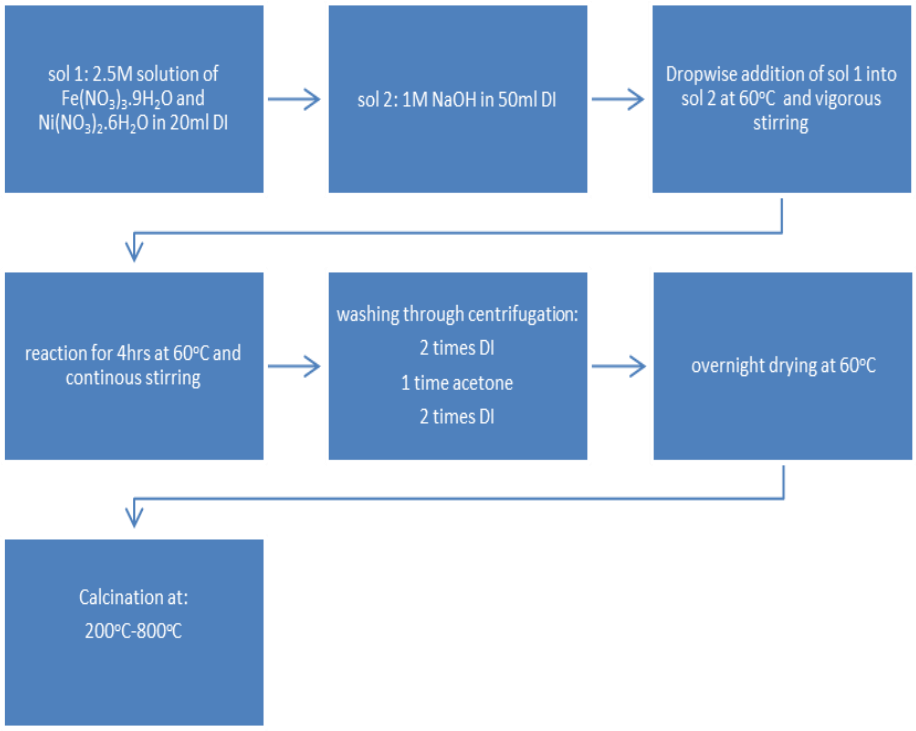

Figure 0-1 Flow chart for the synthesis of NiO-$NiFe_2O_4$ Nanoparticles without Tween

Afterwards, solution 2 was drop wise added in solution 1 which already was maintained at 60°C and was kept for 4 hours at the same temperature and stirring. Later, washing was done by centrifugation. Sample was thoroughly washed two time with DI water, one time with acetone and again two times with DI water. The collected sample was then dried at 60°C overnight in oven and later was calcinated at different temperatures for comparison.

1.16.2 Synthesis of $NiFe_2O_4$ Nanoparticles with Tween

Iron doped NiO NPs (nanoparticles) were prepared by the same procedure as discussed in the above section 4.2.1 but with the addition of surfactant (Tween85). 10ml of the tween was added in 1M NaOH solution in 50ml DI water at 60°C and fast stirring. Solution 2 was prepared exactly as mentioned previously and after drop wise addition in solution 1 was kept at 60°C for 4 hrs. Afterwards, washing, drying and calcination at different temperatures was also performed similarly.

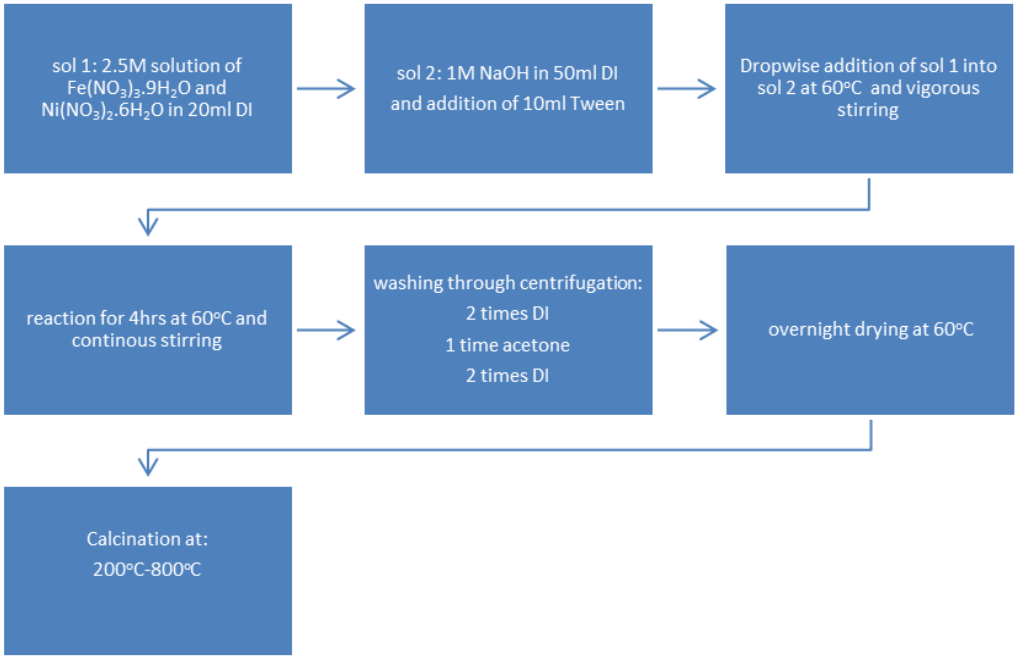

Figure 0-2 Synthesis of NiO-$NiFe_2O_4$ Nanoparticles with Tween

1.16.3 Functionalization of MWCNTS (Multiwalled Carbon Nanotubes)

Multiwalled Carbon nanotubes were functionalized using acidic approach. 0.65g of the CNTs were added into 15ml mixture of concentrated acid HNO_3/H_2SO_4 (1/3 v/v) and was sonicated for half an hour. In an oil bath with temperature of 90^oC, the dispersed mixture was suspended and was refluxed for 7.5 hrs under continuous stirring. Neutralization of the CNTs was then performed by adding 0.1M of NaOH following centrifugation several times with DI water until neutral pH was obtained. Drying was done at 70^oC overnight in oven.

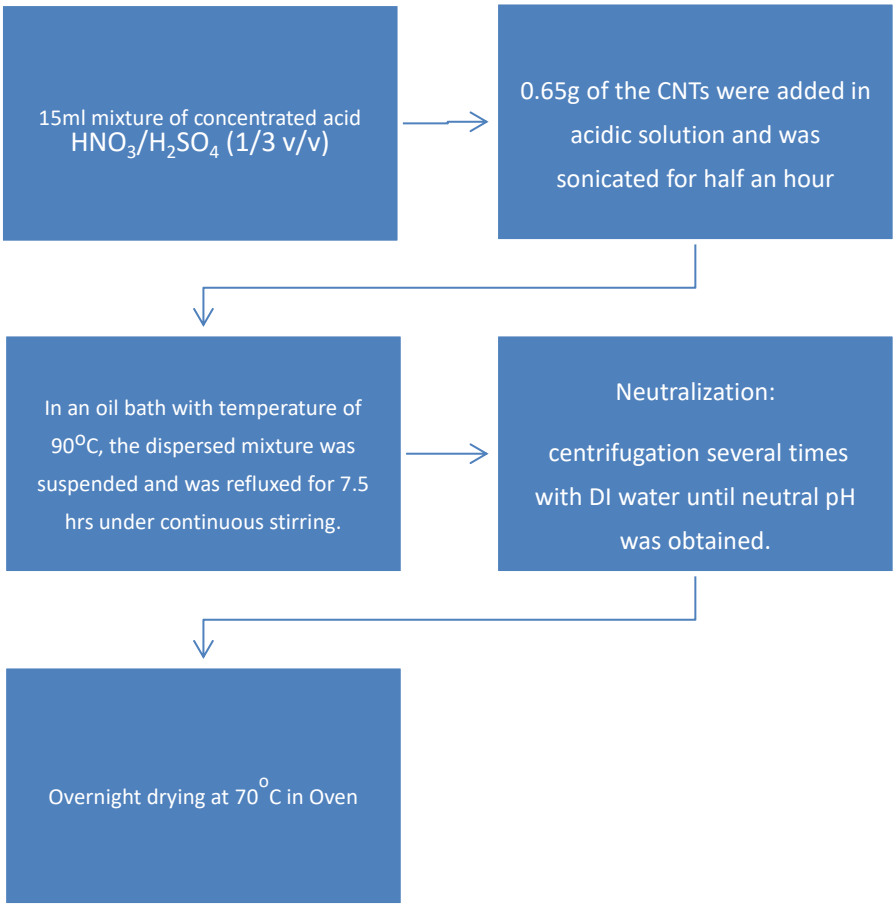

Figure 0-3 Functionalization of MWCNTS (Multiwalled Carbon Nanotubes)

1.16.4 Formation of NiO-$NiFe_2O_4$/ functionalized MWCNTs Nanocomposites

Composite of synthesized Nickel iron oxide NPs was prepared with functionalized CNTs by physical rout. Composites with different proportions of CNTs (5%, 10%, 15% and 20%) were prepared by making dispersion in 10ml of DI water. Dispersion was done by sonication at ambient temperature for 16hrs. Afterwards, drying at 60°C overnight in oven and grinding in mortar pestle for more than an hour was done and resultantly nanocomposites were obtained.

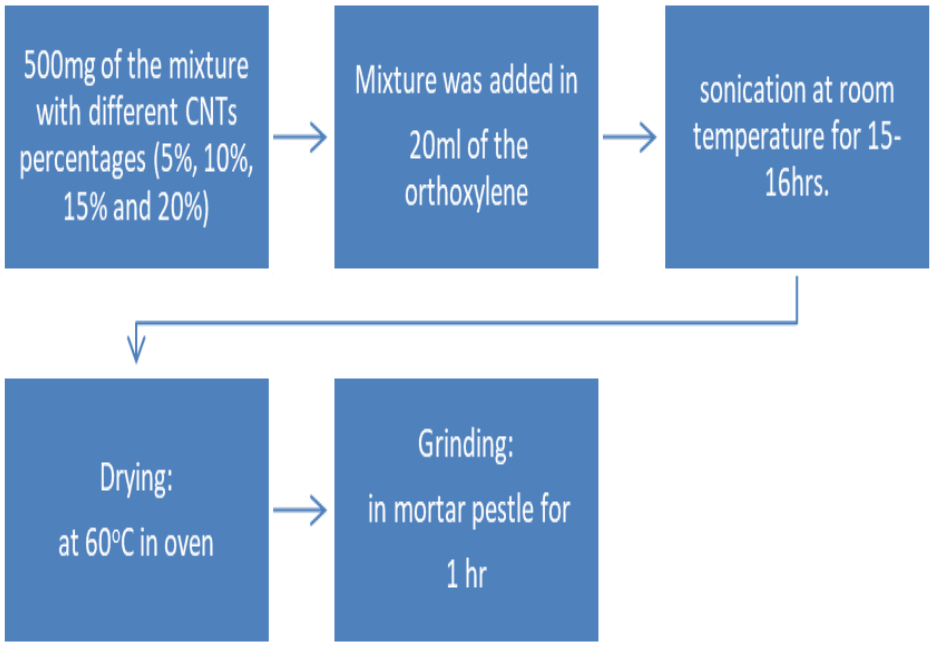

Figure 0-4 Formation of NiO-$NiFe_2O_4$/ functionalized MWCNTs Nanocomposites

1.16.5 Preparation of Anode

Anode was prepared for electrochemical water splitting. For preparation of anode 2mg of the sample was poured into 1ml solution of DI and ethanol in 2:1 respectively. For 2:1 solution of DI:ethanol, 320 µl of the ethanol was poured into 680µl of distilled water (DI). 30µl of Nafion was also poured as a binder. The solution was then sonicated for 1hr in a bath sonicator. With the help of micropipette 5µl of the mixture was then drop casted on a cleaned GC (glassy Carbon) electrode. The electrode was then left overnight for drying at ambient temperature.

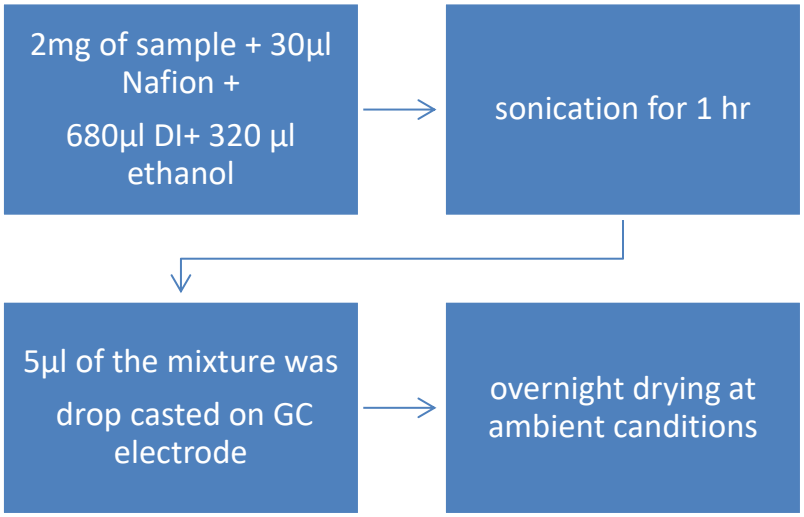

Figure 0-1 Preparation of Anode

CHAPTER 5

Results and discussions

1.17 X-Ray Diffraction (XRD)

X-ray diffraction was performed for the confirmation of the desired structure and investigation of crystallographic properties of the synthesized nanoparticles. Testing was performed at room temperature using STOE powder X-rays Diffractometer. Cu Kα radiations with wavelength 0.154nm were used for diffraction and scanning rate was chosen from 5^o to 85^o. X-ray diffraction of the nanoparticles synthesized via co-precipitation approach in the presence of surfactant tween, without tween and their composites with MWCNTs were performed.

1.17.1 NiO-$NiFe_2O_4$ without Tween

Fig 5.1 exhibits the XRD graph of the NiO-$NiFe_2O_4$ Nanoparticles synthesized in the absence of tween calcinated at different temperatures for 3hrs. No well-defined peaks were obtained for the particles calcinated below 600^oC which depicts that the formation of the phase starts at 600^oC below this temperature structure is amorphous and no crystalline phase is formed.

Diffraction peaks at $2\theta = 18^o$ (111), 30^o (220), 35.4^o (311), 37^o (222), 43^o (400), 53.5^o (422), 57^o (511), 62.7^o (440), 70.7^o (620), 73.9^o (533) and 79^o (444) were obtained. The obtained peaks with specified hkl planes assured the formation of cubic structure of $NiFe_2O_4$ with JCPDS Card No.01-088-0380. Whereas, peaks around 37^o (111), 43^o (200), 62.7^o (220) and 79^o (222) confirms the formation of NiO phase with JCPDS Card No 847-1049. No extra peaks due to impurity were found depicting the absence of significant amount of any kind of impurity.

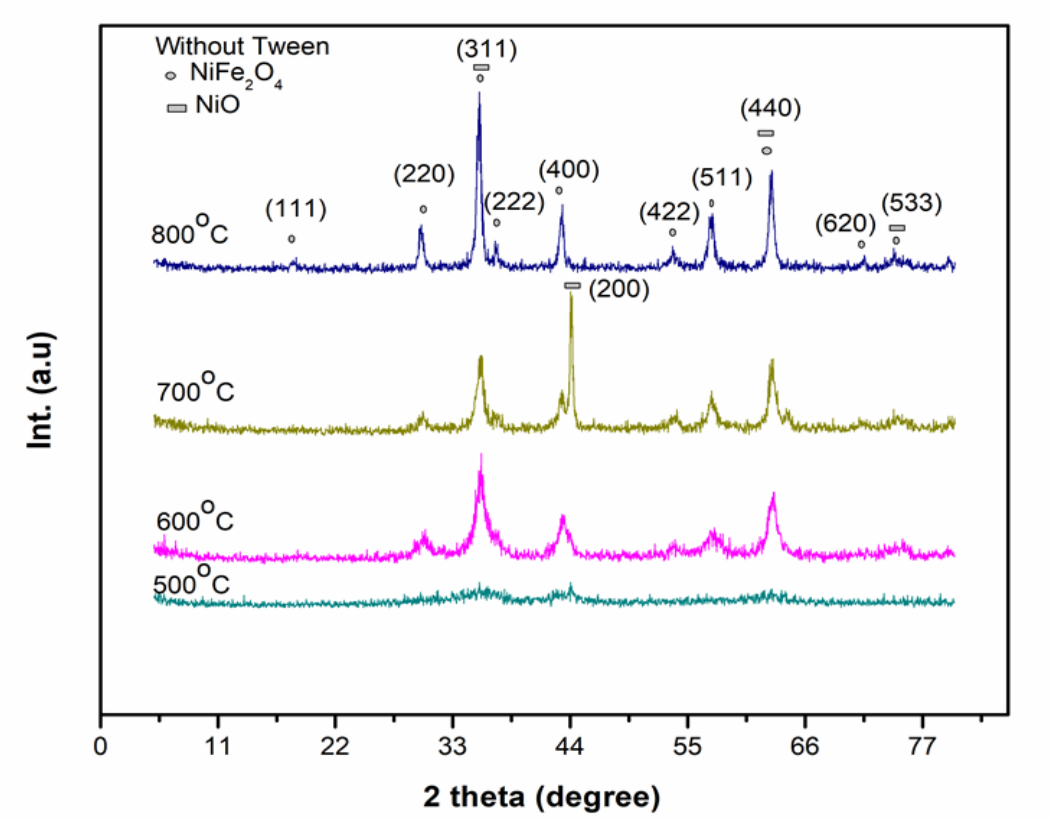

Figure 0-1 XRD pattern of $NiFe_2O_4$ without Tween

Another factor to be observed in the graph is that, with increasing temperature from bottom to top the peak intensity in increasing and the width is decreasing. This is due to the increasing crystallite size with increase in temperature as, increase in temperature causes increase in crystallite size. Another factor can also be considered here. As at 800°C NiO phase (which is more dominant at 700°C) is vanishing. This may also cause the increase in crystallite size as, hybrids and doping always cause the reduction of crystallite size.

1.17.2 NiO-$NiFe_2O_4$ with Tween

Fig 5.2 exhibits the XRD graph of the sample prepared by the same procedure except the addition of surfactant Tween 80 at the time of synthesis via co-precipitation. Same XRD pattern is obtained as is obtained in the previous case (without Tween).

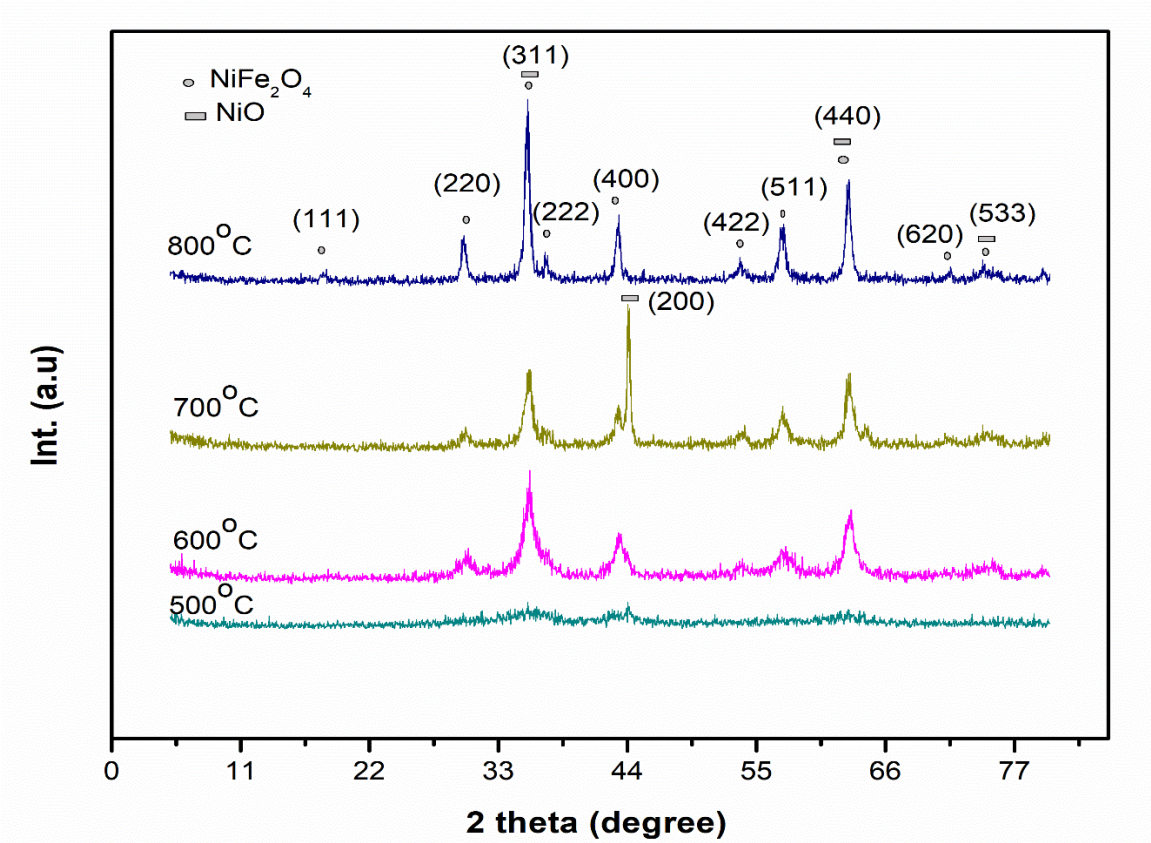

Figure 0-2 XRD pattern of NiO-$NiFe_2O_4$ with Tween

Similar to aforementioned Nickel Iron Oxide, peaks at 2θ= 18° (111), 30° (220), 35.4° (311), 37° (222), 43° (400), 53.5° (422), 57° (511), 62.7° (440), 70.7° (620), 73.9° (533) and 79° (444) were obtained. The obtained peaks with specified hkl planes assured the formation of cubic structure of $NiFe_2O_4$ (JCPDS Card no.01-088-0380) and no extra peaks due to impurity were found. Nor any peak shift is observed. Whereas, peaks around 37° (111), 43° (200), 62.7° (220) and 79° (222) confirms the formation of NiO phase with JCPDS Card no 847-1049. Similar to the previous case, no extra peaks due to impurity were found depicting the absence of significant amount of any kind of impurity.

Again as mentioned for previous case of particles in the absence of tween, with increasing temperature from bottom to top the peak intensity is increasing and the width is decreasing in this case too. This again is due to the increased crystallite size with increasing temperature. As increase in temperature causes increase in crystallite size.

Another factor can also be considered here. As at 800°C NiO phase (which is more dominant at 700°C) is vanishing. This may also cause the increase in crystallite size as, hybrids and doping always causes the reduction of crystallite size.

1.17.3 NiO-$NiFe_2O_4$/Multi walled CNTs Composites

NiO-$NiFe_2O_4$/MWCNTs composites with different MWCNTs percentages (5%, 10%, 15% and 20%) were later formed and their x-ray diffraction analysis was performed. Fig 5.3 manifests the comparison of XRD pattern of pure NiO-$NiFe_2O_4$ and NiO-$NiFe_2O_4$/ MWCNTs 20% (highest percentage among composites). Diffraction peaks at 2θ= 18° (111), 30° (220), 35.4° (311), 37° (222), 43° (400), 53.5° (422), 57° (511), 62.7° (440), 70.7° (620), 73.9° (533) and 79° (444) were obtained for, pure NiO-$NiFe_2O_4$ and NiO-$NiFe_2O_4$ /MWCNTs composite.

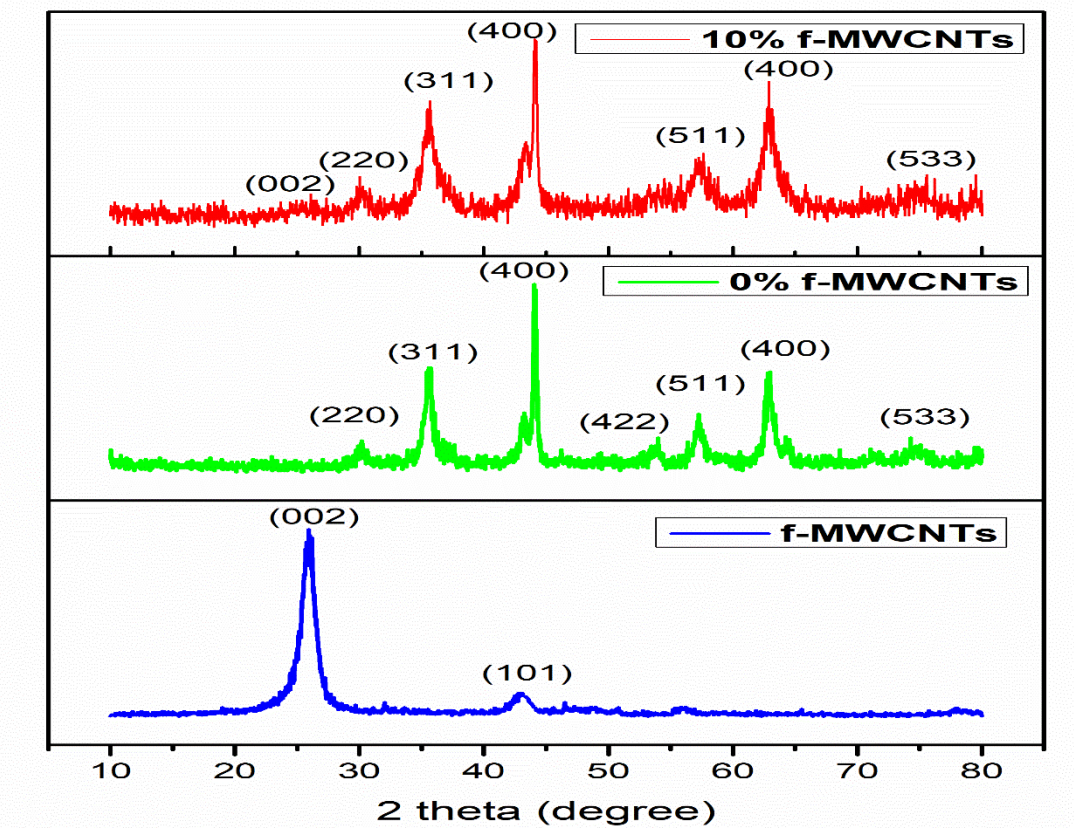

Figure 0-3 comparison of pure NiO-$NiFe_2O_4$ and NiO-$NiFe_2O_4$ / f-MWCNTs 10%

Only a small negligible peak extra peak was obtained around 26° with plan (200) which can be attributed to uniform distribution and anchoring of NiO-$NiFe_2O_4$ and CNTs and

the presence of CNTs in very small quantity of CNTs in comparison to NiO-$NiFe_2O_4$. Also a slight change in the FWHM can be observed. CNTs incorporation increases FWHM slightly which can to attributed to the introduction of impurity due to CNTs and reduction of crystallite size. This comparison also shows that no phase change occurs in case of formation of CNTs composite via physical rout.

Table 0-1 variation of crystallite size with calcination temperatures for Samples without surfactant

Calcination Temperature	**600°C**	**700°C**	**800°C**
Crystallite Size (nm)	18.21	20.8	45.48

Table 0-2 variation of crystallite sized with increasing temperature for sample with surfactant

Calcination Temperature	**600°C**	**700°C**	**800°C**
Crystallite Size (nm)	13.82	18.47	31.6

Table 0-3 variation of crystallite size with increasing MWCNTs concentration

MWCNTs Percentage	**0%**	**10%**	**20%**
Crystallite Size (nm)	18.47	14.28	11.37

Crystallite sizes of the samples were calculated using Debye's scherrer formula. The aforementioned table clearly shows the variation of crystallite size with varying parameters. Both the samples (prepared in the presence and absence of surfactant) are

showing increase in crystallite size with increasing temperature. But it can be observed that the particles with Tween have lower crystallite sizes comparing to the particles prepared in the absence of surfactant.

Three major parameters are essential to be considered here.

1) Samples prepared in the presence of Surfactant (Tween 85) show smaller crystallite size comparing to sample prepared in the absence of surfactant. The smaller crystallite sizes in the presence of surfactant are attributed to the amphiphilic nature of surfactant which controls the size of nanoparticle by capping. Capping reduces surface energy which results in controlled growth.

2) Other trend that can be noticed in the table is that increasing calcination temperature increases crystallite size due to Ostwald ripening, which is also prominent by XRD patterns. As at higher temperatures the peaks are sharper, showing more crystallinity and increase in crystallite size.

3) Incorporation of MWCNTs reduces the crystallite size from 18.47nm to 14.28nm for 10% MWCNTs incorporation. Which is due to the fact that introduction of MWCNTs cuts the grains by creating networks within and outside the grain boundaries.

1.18 Fourier Transform Infrared Spectroscopy (FTIR)

To figure out the presence of certain functional groups in samples FTIR were performed in the range of 400-4000cm^{-1}. All the FTIR tests were performed at room temperature. Samples for FTIR were prepared in the form of pallets using KBr as transparent dye. The pallets were formed in hydraulic press by applying pressure of 5 tons for 3 minutes.

1.18.1 FTIR spectrum of NiO-$NiFe_2O_4$ NPs prepared with Tween

In Fig 5.4 the FTIR spectrum of NiO-$NiFe_2O_4$ sample is shown which was prepared by co-precipitation in the presence of Tween 80. The upper and lower spectra in this figure shows sample (prepared with Tween) with and without calcination respectively. Various peaks with different wavenumbers were obtained depicting the presence of certain functional groups. The broad peak around 3500cm^{-1} is due to the stretching vibration of hydroxyl group of water. The peaks around 2924cm^{-1} and 2796cm^{-1} are due

to the presence of CH_2 and C-H bonds respectively, whereas peaks around 1560cm^{-1} and 1397cm^{-1} are due to C=C/C=O and CH_3 respectively.

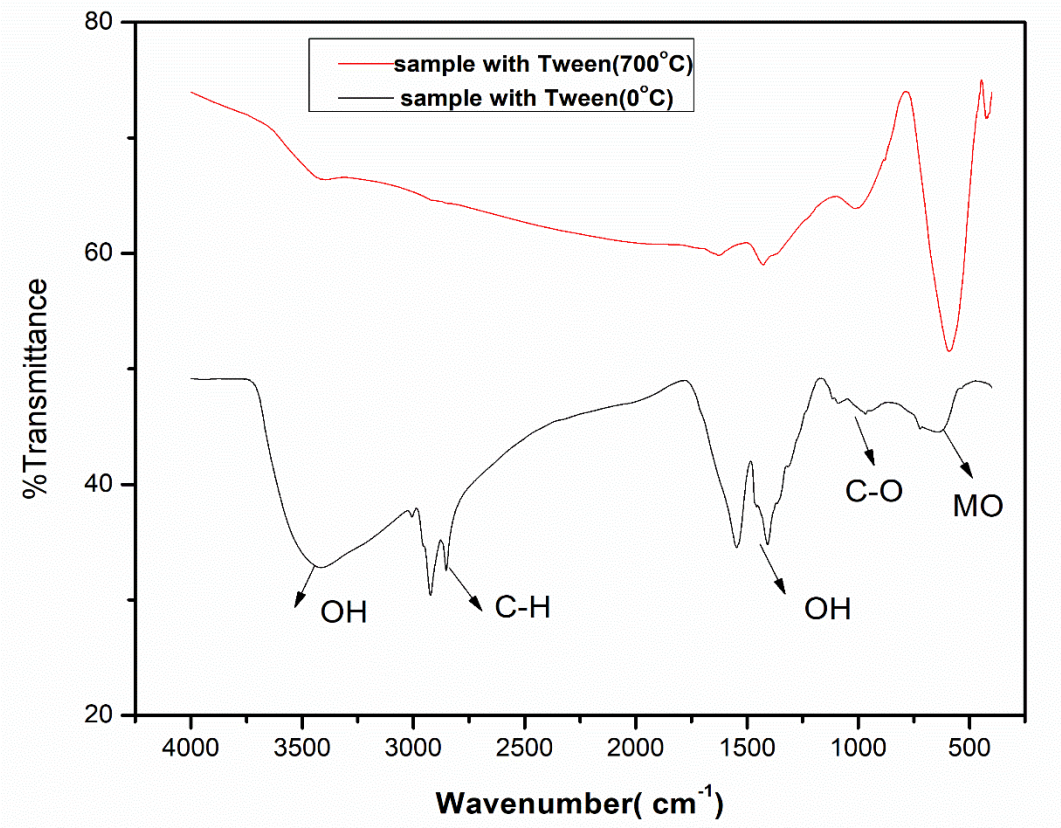

Figure 0-4 FTIR comparison spectrum of NiO-$NiFe_2O_4$ prepared with Tween

Peaks around 1100cm^{-1} and 955cm^{-1} are due to C-O and C-C bonds respectively. While, peak at 623cm^{-1} indicates the presence of metal oxide. It is clear from the spectrum that the freshly prepared sample contains a huge amount of water which after calcination (at 800^oC) diminishes. Similarly, the peaks of various organic functional groups e.g. CH_2, C-H, C=C, C=O, CH_3, C-O and C-C are due to the surfactant (Tween 80) which also diminish after calcination as at higher temperature surfactant is removed. Another important aspect to be noticed is that, without calcination no proper metal Oxide phase is formed. While there is a prominent peak of metal oxide after calcination which exhibits that after calcination the proper metal oxide phase is formed.

1.19 Brunauer, Emmett and Teller (BET)

BET analysis of the nanoparticles synthesized in the presence and absence of surfactant shows a significant difference in their surface areas and pore sizes.

Table 0-4 comparison of surface area and porosity of different synthesized adsorbents

Adsorbant	T600^{O}C	T700^{O}C	T800^{O}C	WT800^{O}C
BET surface area (m^2/g)	50.95	23.06	18.37	13.86
Pore size (nm)	35.75	76.61	124.49	17.43

Pore size of the material is showing an increasing trend with increasing temperature which is due to the removal of surfactant at higher temperatures. Whereas, the adsorbent prepared in the absence of surfactant is even showing lower pore size of 17.43nm comparing to the adsorbent prepared in the presence of surfactant, which has pore size of 124.49.

Table 0-5 comparison of surface area and porosity of composite adsorbents

Adsorbant	0% MWCNTs	10% MWCNTs	20% MWCNTs
BET surface area (m^2/g)	23.06	77.47	70.47
Pore size (nm)	76.61	63.73	12.36

While in case of the incorporation of MWCNTs in the sample the pore size is decreasing as it has started filling the pores. On the other hand, surface area of the adsorbent has shown an increase with incorporation of MWCNTs because of the higher surface areas. But upon further increase in the percentage of the MWCNTs surface area has shown a decline in surface area. The possible reasons for this might be filling of pores.

Another factor to be considered in the table is that increasing temperature is though increasing pore size but at higher temperature surface area is decreasing due to increase in particle size.

Figure 5-5 shows the trend of surface area with increasing temperature in the case of sample prepared in the presence of surfactant (Tween). The decreasing surface area with increasing temperature can be justified by the fact that the increase in temperature increases crystallite size which reduces surface area.

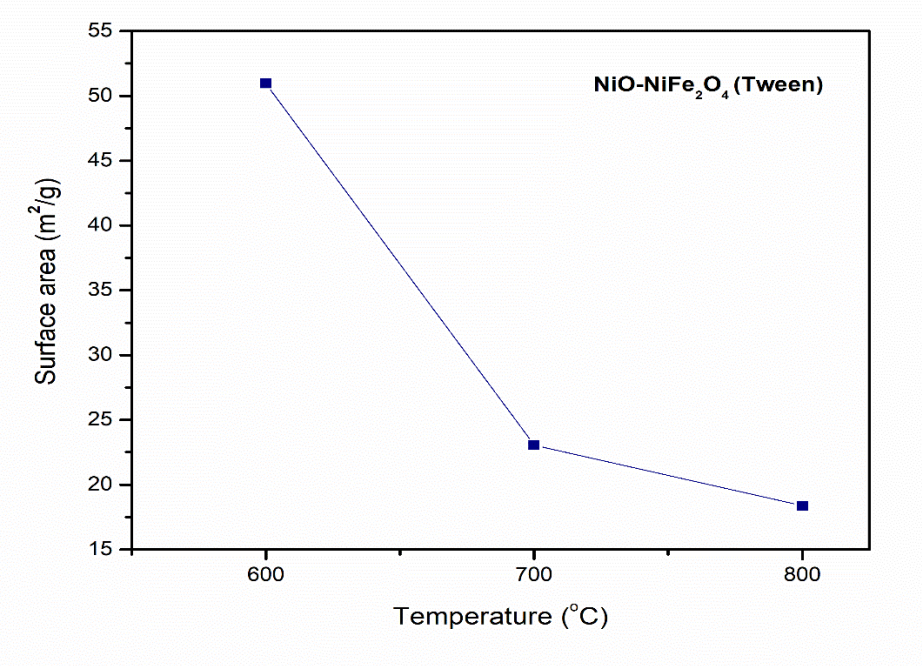

Figure 0-5 Trend of Surface area with increasing temperature for $NiO\text{-}NiFe_2O_4$ (Tween)

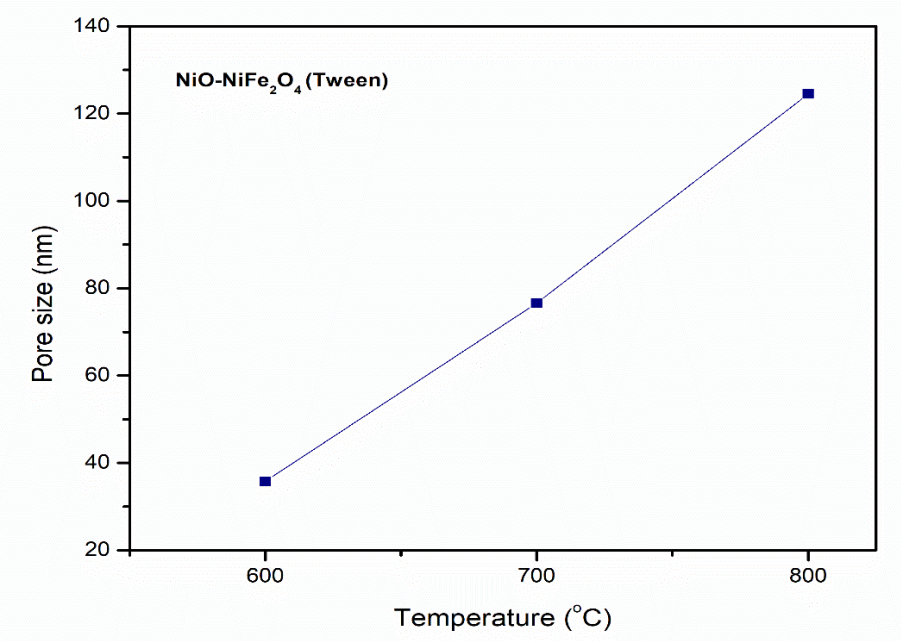

Figure 0-6 Trend of pore size with increasing temperature for $NiO\text{-}NiFe_2O_4$ (Tween)

Figure 5-6 shows the increase of pore size with increase in temperature. As the temperature is increased the pore size is increased due to the removal of surfactant.

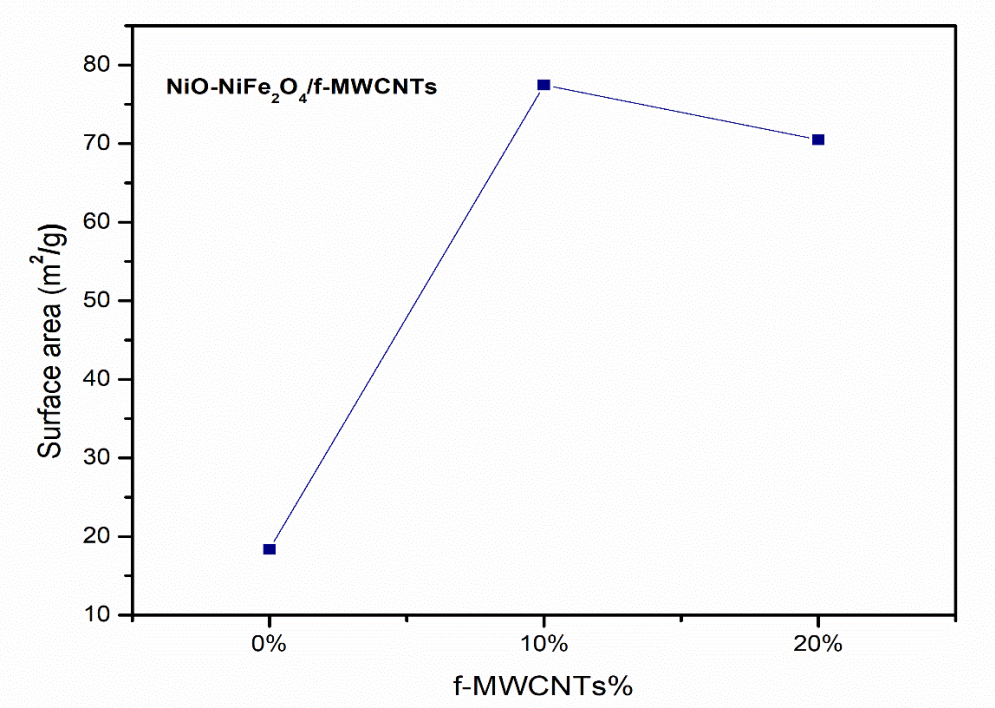

Figure 0-7 Trend of Surface area with increasing MWCNTs concentration for NiO-$NiFe_2O_4$/f-MWCNT Nano-composites

Figure 5-7 shows the trend of surface area with increasing MWCNTs concentration in Nano-composite. At start surface area increases with increasing concentration due to the high surface to volume ratio of CNTs. But upon further increase after 10%, surface area started decreasing. This decrease might be due to the filling of pore as at further increase the amount of CNTs increase significant enough to fill the pore and filling of pores has started decreasing the surface area or we can say the cumulative pore sizes of the MWCNTs and the particles. Figure 5-8 is showing the decrease of pore size with increasing concentration of CNTs.

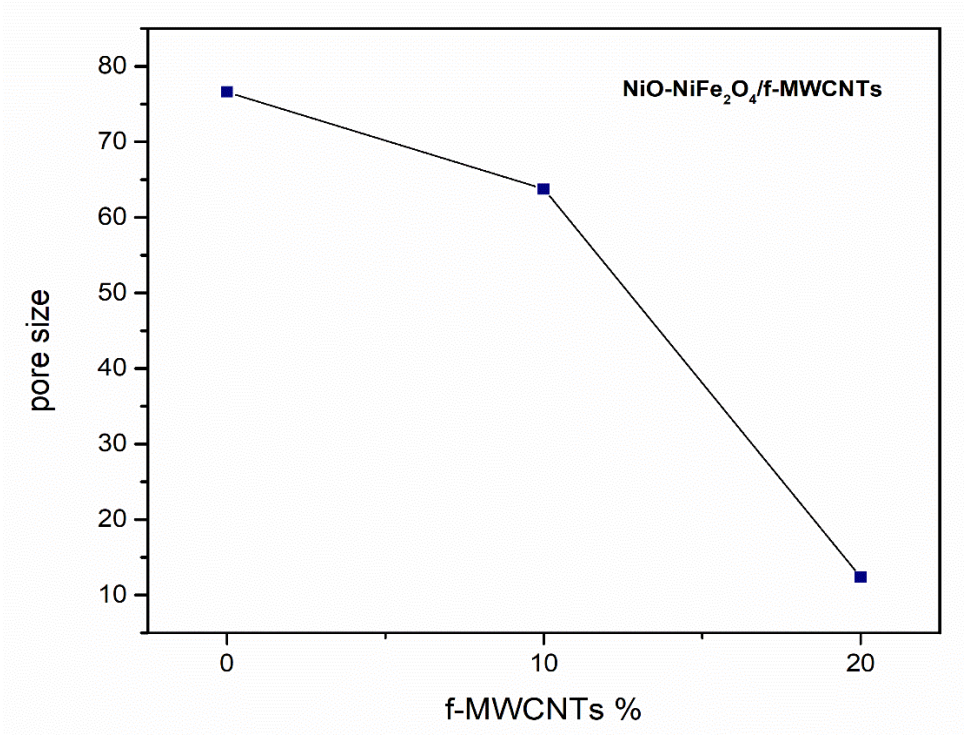

Figure 0-8 Trend of pore size with increasing MWCNTs concentration for NiO-$NiFe_2O_4$/f-MWCNT Nano-composites

1.20 Scanning Electron Microscopy (SEM)

All the samples for scanning electron microscopy were prepared by forming suspensions of the samples in DI water. For fine suspensions, samples were sonicated for 3hrs at ambient temperature following drop casting on thoroughly cleaned glass/ ITO slides and later were air dried. Later, samples were ion sputtered using JEOL JFC-1500, to form a thin gold layer. Scanning Electron Microscopy was then performed with 20kV of accelerating voltage in JEOL JSM 6490 (LA) instrument.

1.20.1 SEM analysis of NiO-$NiFe_2O_4$ Nanoparticles:

Figure 5-9 shows the SEM images of NiO-$NiFe_2O_4$ nanoparticles prepared with surfactant and calcination at 700^oC at different magnifications.

(a)

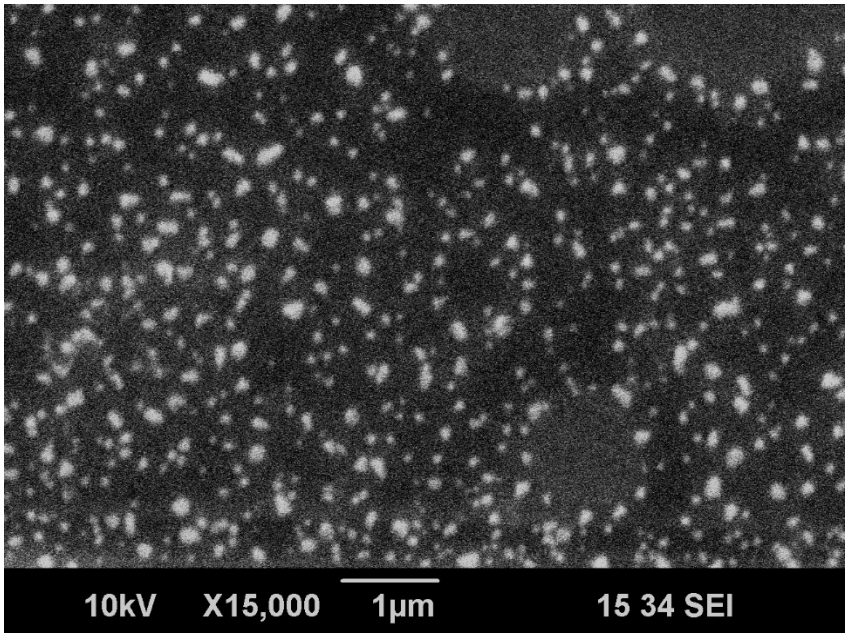

(b)

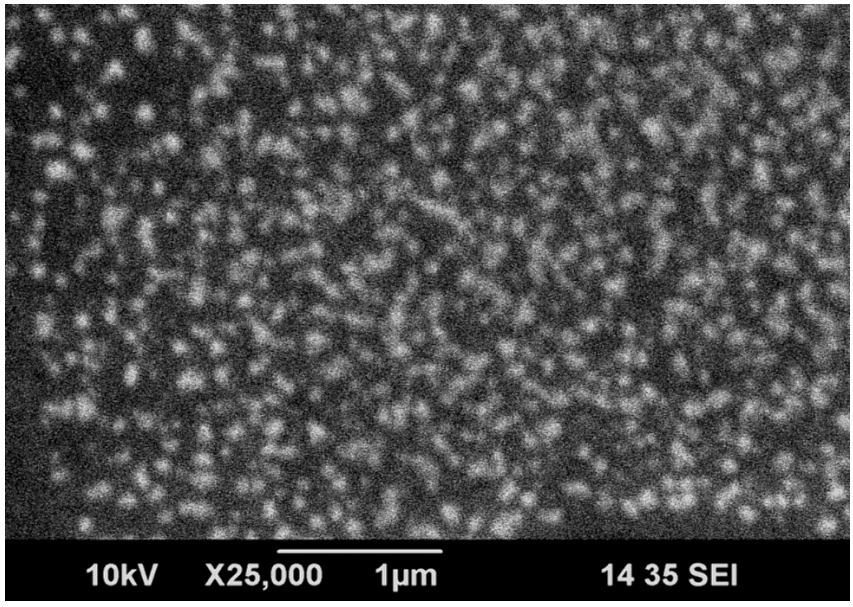

Figure 0-9 SEM images of NiO-$NiFe_2O_4$ nanoparticles (prepared with surfactant, calcination at 700^{o}C) at different magnifications

1.20.2 SEM analysis of NiO-NiFe2O4/f-MWCNTs Nano-composite:

In Figure 5-10 SEM images of the acid treated MWCNTs are shown. No distortion of the MWCNTs structure has occurred as can be seen after acid treatment.

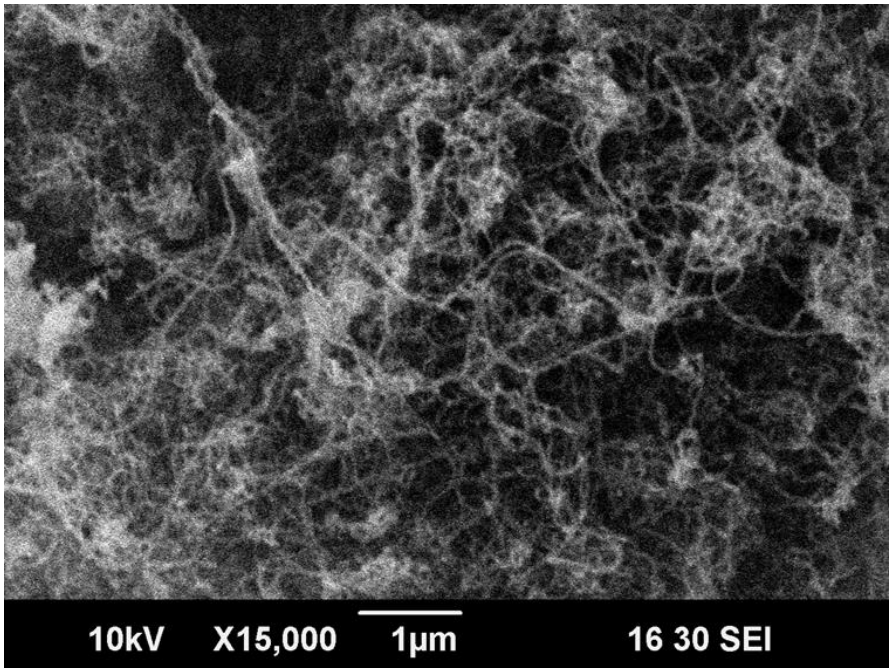

(a)

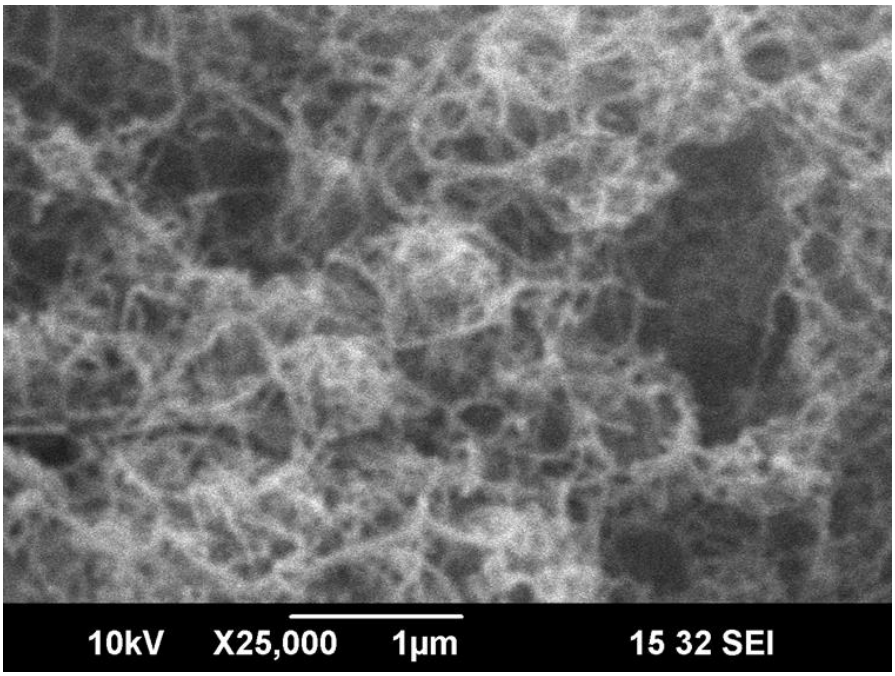

(b)

Figure 0-10 SEM images of f-MWCNTs

In Figure 5-11 SEM images of nanocomposits of the $NiO\text{-}NiFe_2O_4$ and functionalized MWCNTs with 10% MWCNTs concentration are shown.

(a)

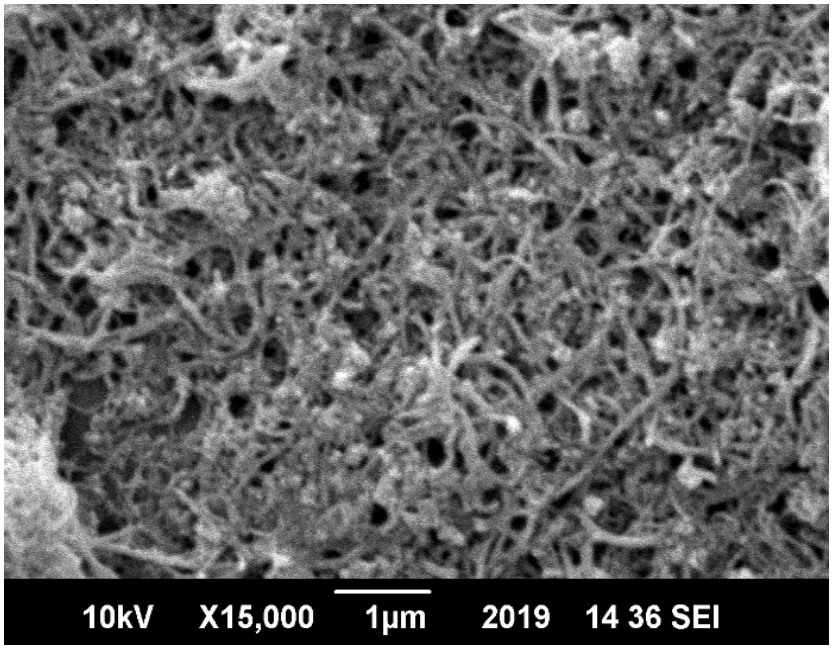

(b)

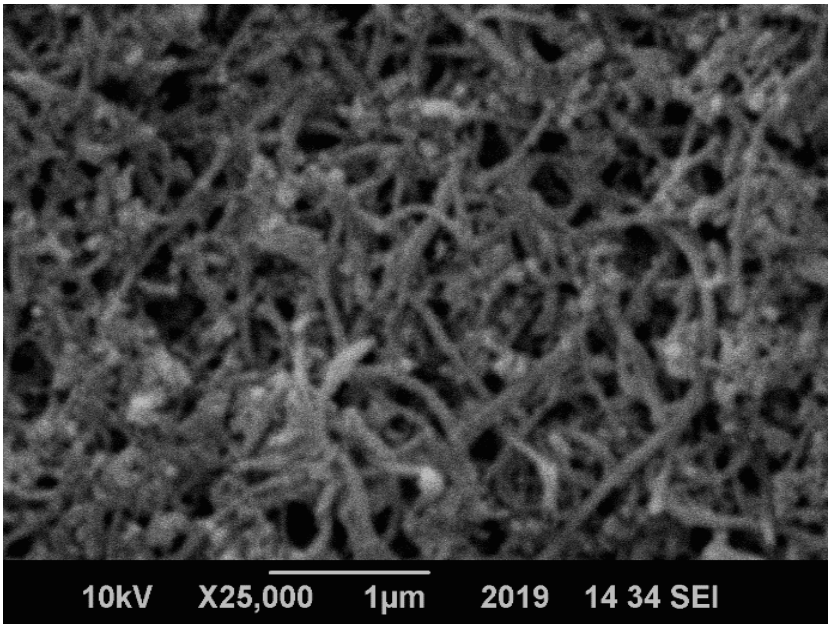

Figure 0-11 SEM images of $NiO\text{-}NiFe_2O_4$/f-MWCNTs nanocomposite with 10% f-MWCNTs at different magnifications

The point to be observed is that, the nanoparticles are dispersed/ decorated onto CNTs uniformly without any significant agglomeration. But a little agglomeration is still formed which can be attributed to the extremely magnetic nature of Nickel Iron oxide nanoparticles. Usually poor sonication is also a significant factor for non-uniform dispersion but that doesn't seem major reason in this case as sonication for more than 16hrs was done in this case. From the following Figures it can also be seen that after acid treatment for functionalization of MWCNTs, the structure of the MWCNTs is not distorted.

1.21 Contact angle measurement:

To confirm the functionalization of the MWCNTs contact angle measurement was conducted. For comparison pristine and functionalized CNTs were dispersed in DI and were drop casted on glass slides to form coating. Later contact angle measurement was performed by using Kruss power drop analyszer. From the following Figure the difference of contact angles for both is prominent. Pristine CNTs are hydrophobic so, they have greater angles. Whereas, the functionalized CNTs have become hydrophilic so their contact angles are significantly small.

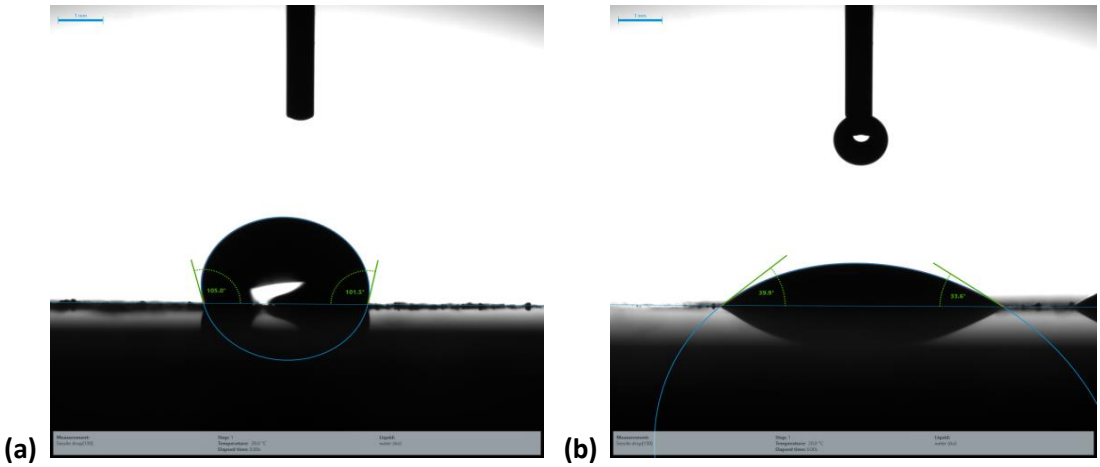

Figure 0-12 (a) Contact angle of pristine CNTs (b) contact angle of functionalized CNTs

1.22 Dispersibility test:

Dispersibility test of functionalized and pristine CNTs was performed by making dispersion of both CNTs Types in DI by sonicating for 15min and then leaving for prolonged time. Functionalized CNTs were supposed to form good and long lasting dispersion comparing to pristine CNTs, due to its hydrophilicity and so it did, as is shown in the following figure. This hydrophilicity is attributed to the introduction of polar groups at the surface of CNTs as a result of acid treatment functionalization.

Figure 0-13 Dispersion of functionalized and pristine CNTs at left and right respectively

1.23 Electrochemical Testing:

Electrochemical testing was performed by gamry setup of electrochemical workstation. Cyclic voltammetry (CV) was performed for this purpose over the potential window of 0.5 to 1.8V. Three-electrode system was used for current measurement over changing voltage. Synthesized electro-catalyst deposited over GC (glassy carbon) electrode was used as working electrode. Whereas, Platinum (Pt) and silver-silver chloride (Ag/AgCl) were used as counter and reference electrodes respectively. 0.1M KOH solution was used as electrolyte in which all the three electrodes were dipped. For comparison CVs of all the samples (including samples with and without surfactant, calcinated at different

temperatures and their composites with functionalized MWCNTs at different concentrations) were performed at different scan rates.

1.23.1 CV comparison of NiO-$NiFe_2O_4$ without Tween

Cyclic voltammetry of the Fe doped NiO Nps synthesized in the presence of the surfactant (Tween 85) were performed for comparison of the prepared samples at different calcination temperatures (600^oC, 700^OC and 800^oC). As IV curves depict that the sample calcinated at 700^oC outperforms the other two samples, calcinated at 600^oC and 800^oC.

Samples calcinated at 600^oC, 700^oC and 800^oC show 10.5mA/cm^2, 15mA/cm^2 and 8mA/cm^2 of current densities respectively. Obtained CV results are supported by XRD results. Following might be the reasons for this trend:

- ✓ At 700^oC a prominent hybrid phase of NiO-$NiFe_2O_4$ is formed as can be seen by XRD graph which shows a prominent peak of NiO at 700^oC. This more prominent NiO phase in NiO-$NiFe_2O_4$ might be one of the reasons for its outperformance. As NiO is believed to be more efficient and active OER catalyst in NiO-$NiFe_2O_4$ hybrid. Whereas, Fe is introduced to increase conductivity.[77]
- ✓ Another factor which can be considered here regarding hybrid phase formation is that hybrids are believed to be more active comparing to single phases because for of their grain boundaries and hence improved activity.
- ✓ On the other hand it can be seen that sample at 600^oC showed better results than samples at 800^oC. This can be justified by the Table 5-1. As at higher temperature the crystallite size is increasing it means that surface area is decreasing which reduces its activity. So the sample at 600^oC showed better results due to their smaller crystallite size comparing to 800^oC with higher crystallite size.

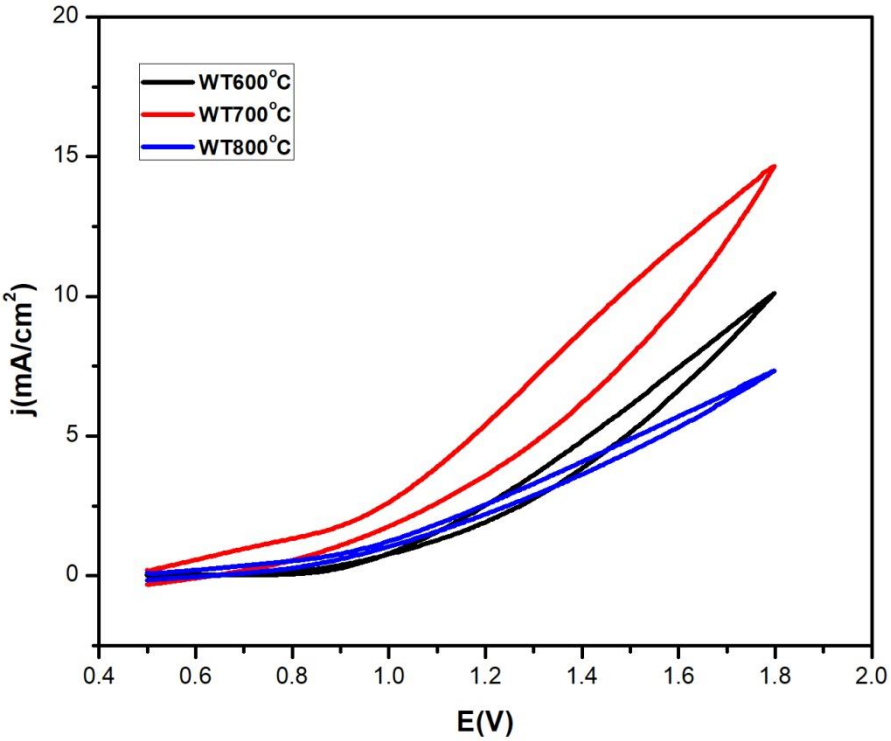

Figure 0-14 CV comparison of NiO-$NiFe_2O_4$ (without Tween) at different calcination

1.23.2 CV comparison of NiO-$NiFe_2O_4$ with Tween

Similar to the previous case CVs of porous samples prepared in the presence of Surfactant at different temperatures were performed for comparison. Similar to the comparison for samples without surfactant, IV curves of porous samples exhibit that the sample calcinated at 600°C outperforms the other two samples, calcinated at 700°C and 800°C but in this case with more current densities comparing to the non-porous samples.

Samples calcinated at 600°C, 700°C and 800°C show 16mA/cm^2, 19mA/cm^2 and 14mA/cm^2 of current densities respectively. Obtained CV results are supported by the XRD and BET results in the following ways:

- ✓ Similar to the previous case 700°C showed better current density values which again can be attributed to the formation of NiO-$NiFe_2O_4$ at this temperature which can also be observed by the XRD graphs of these samples. And also that as mentioned earlier NiO is believed to be more efficient and active OER catalyst. And also that the hybrids are believed to be more active comparing to single phases due to their grain boundaries and hence improved activity.

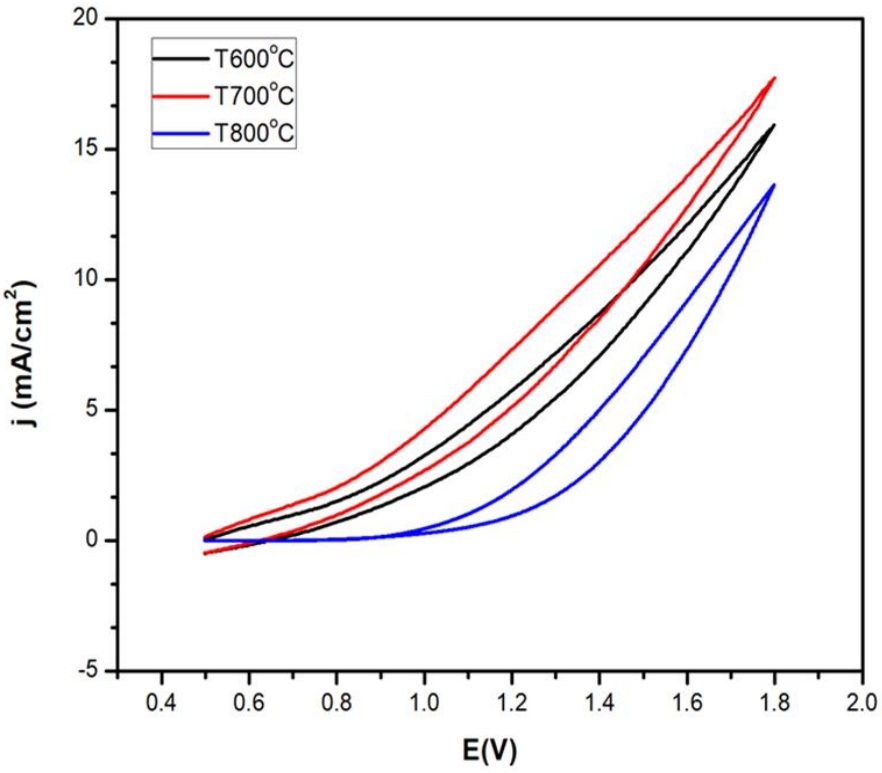

Figure 0-15 CV comparison of NiO-$NiFe_2O_4$ (Tween) at different calcinations

- ✓ Whereas, in resemblance to previous case the samples at 600°C also showed better results comparing to 800°C. This can be justified by both the XRD and BET results from Table 5-1 and Table 5-2. Higher

temperature results increased crystallite, size lower surface area and hence reduced activity.

- ✓ Another factor to be observed is that samples synthesized in the presence of surfactant has shown better performances than the previous case (in the absence of surfactant) which also can be justified by the BET and XRD results. As samples prepared in the presence of Tween have lower crystallite sizes and pores leading to better activity and performances comparing to the samples in the absence of surfactant.

1.23.3 CV comparison of NiO-$NiFe_2O_4$/ f-MWCNTs composites

As in all the above mentioned sample types (With Tween 600°C-800°C and Without Tween 600°C-800°C), porous sample prepared in the presence of Tween and calcinated at 700°C showed the best performance therefore this sample was chosen for the formation of their composite with functionalized MWCNTs.

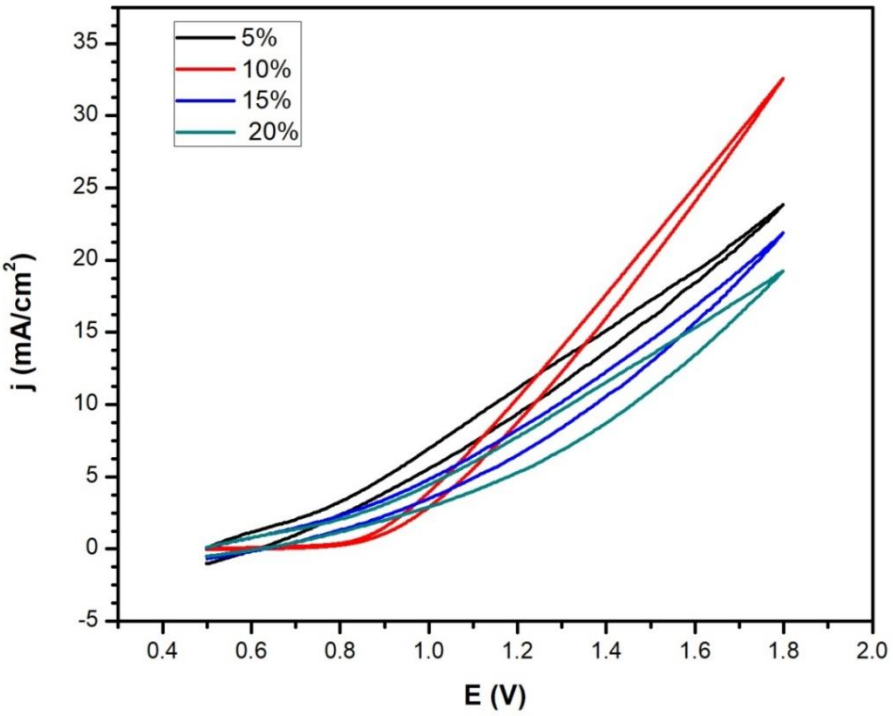

Figure 0-16 CV comparison of NiO-$NiFe_2O_4$/f-MWCNTs composites at different concentrations

Later their CV was performed to examine their efficiency and comparison of different doping concentrations (5%, 10%, 15% and 20%).

As exhibited by the IV curve the Samples with 5%, 10%, 15% and 20% showed 25A/cm^2, 35mA/cm^2, 22mA/cm^2 and 20mA/cm^2 of current densities respectively. Obtained CV results are supported by the the BET results in the following ways:

- ✓ At start, current density of the Nanocomposites increases for 5% and 10% (weight percent) introduction of the f-MWCNTs due to the high surface to volume ratio of CNTs and hence greater activity of sample upon introduction of MWCNTs as supported by BET surface area results.
- ✓ But at higher concentrations 15% and 20% the efficiency is decreased which might be due to the filling of pores as in BET pore size and surface area has shown a decrease in BET results.
- ✓ Another reason for decease at higher concentration might be due to the reason that at higher concentrations of MWCNTs the concentration of NiO-$NiFe_2O_4$ is decreased which was the core catalyst and was responsible for OER (oxygen evolution reaction) whereas, the purpose of introduction of CNTs was just to enhance conductivity and activity due to high surface area.

Conclusions

Synthesis of Fe doped NiO nanoparticles with and without Tween, functionalization of MWCNTs and the fabrication of the composites of synthesized nanoparticles with f-MWCNTs were performed successfully. For the study of fabricated electrocatalysts various characterization techniques including X-Ray diffraction (xrd), Scanning Electron microscopy (SEM), Fourier Transformed Infrared Spectroscopy (FTIR), Brunauer, Emmett and Teller (BET), Contact angle and Cyclic voltammetry (CV) were performed. All the results obtained from these characterizations were analyzed thoroughly for the intended efficiency comparison of all prepared sample types and following conclusions were drawn resultantly.

- Nanoparticles synthesized in the presence of Surfactant showed better performance due to their comparatively smaller particle sizes and porous structure.
- Increasing calcination temperature decreased OER activity of the electrocatalyst due to the increase in particle size and hence lower surface area.
- Nanoparticles at 700^{o}C outperformed the other nanoparticles calcinated at 600^{o}C and 800^{o}C due to the formation of NiO-$NiFe_2O_4$ hybrid phase at this temperature.
- 5% and 10% f-MWCNTs incorporation exhibited significant improvement in electrochemical performance due to the high conductivity and surface area of MWCNTs.
- Further increase of f-MWCNTs incorporation (15% and 20%) showed decreased OER activity due to the reduced percentage of OER (oxygen evolution reaction) active electrocatalyst and reduction in pore size and surface area.

References

[1] I. cera IHS Global Insight, “Energy Transitions: Past and Future,”*United Nations, US Bur. census*., **2013**.

[2] *Special Report Eur 20719,"Hydrogen Energy and Fuel Cell,"European commission, **2003***.

[3] K. W. A. Guy, "*The hydrogen economy"*, Science Direct., Vol. 78, No. 4. **2000**.

[4] D. M. F. Santos and C. A. C. Sequeira, "Hydrogen production through alkaline water electrolysis", “Revisão,” Vol. 36, No. 8, pp. 1176–1193, **2013.**

[5] O. Ellabban, H. Abu-rub, and F. Blaabjerg, “Renewable energy resources : Current status , future prospects and their enabling technology,” *Renew. Sustain. Energy Rev.*, Vol. 39, pp. 748–764, **2014**.

[6] N. S. L. Joshua M. Spurgeon, “Proton exchange membrane electrolysis sustained water vapor,” *Energy Environ. Sci.*, No. 8, **2011**.

[7] K. Im-orb, N. Visitdumrongkul, D. Saebea, Y. Patcharavorachot, and A. Arpornwichanop, “Flowsheet-based model and exergy analysis of solid oxide electrolysis cells for clean hydrogen production,” *J. Clean. Prod.*, Vol. 170, pp. 1–13, **2018**.

[8] J. M. Spurgeon, and N. S. Lewis, “Proton exchange membrane electrolysis sustained by water vapor,” Energy & Environmental Science., pp. 2993–2998, **2011**.

[9] K. Im-orb, N. Visitdumrongkul, and D. Saebea, “Flowsheet-based model and exergy analysis of solid oxide electrolysis cells for clean hydrogen production,” *J. Clean. Prod.*, Vol. 170, pp. 1–13, **2018**.

[10] D. Zeng, K. & Zhang, “Recent progress in alkaline water electrolysis for hydrogen production and applications,” *Prog. Energy Combust. Sci.*, No. 36, pp. 307–326, **2010**.

[11] P. Sanchis and M. Gandia, “Hydrogen production from Water Electrolysis : Current Status and Future Trends,” IEEE., Vol. 100, No. 2, **2012**.

[12] P. E. Lower, “The Nernst Equation,” *LibreText*, **2019**.

[13] K. Zeng and D. Zhang, “Recent progress in alkaline water electrolysis for hydrogen production and applications,” *Prog. Energy Combust. Sci.*, Vol. 36, No. 3, pp. 307–326, **2010**.

[14] S. Lower, “CHEM1 VIRTUAL TEXTBOOK.”,**2010**.

[15] Z. Wang and L. Wang, “SPECIAL ISSUE : Advanced Materials for

Photoelectrochemical Cell Photoelectrode for water splitting : Materials, fabrication and characterization," Science China Materials., Vol. 61, No. 6, pp. 806–821, **2018**.

[16] H. Dau, C. Limberg, T. Reier, M. Risch, and S. Roggan, "The Mechanism of Water Oxidation : From Electrolysis via Homogeneous to Biological Catalysis," Chemistry Europe., pp. 724–761, **2010**.

[17] C. V Jacques, "Heterogeneous Catalysis on Metal Oxides," Catalysts., Vol. 11, No.7, pp. 341, **2017**.

[18] M. G. Walter *et al.*, "Solar Water Splitting Cells," ACS., Vol. 110, No. 11, pp. 6446–6473, **2010**.

[19] C. K. Mavrokefalos and G. R. Patzke, "Water Oxidation Catalysts : The Quest for New Oxide-Based Materials," Inorganics., Vol. 7, No. 3, **2019**.

[20] N. Danilovic *et al.*, "Activity-stability trends for the oxygen evolution reaction on monometallic oxides in acidic environments," *J. Phys. Chem. Lett.*, Vol. 5, No. 14, pp. 2474–2478, **2014**.

[21] A. Eftekhari, "Tuning the electrocatalysts for oxygen evolution reaction," *Mater. Today Energy*, Vol. 5, pp. 37–57, **2017**.

[22] N. Kim, Y. J. Sa, S. Cho, I. So, and K. Kwon, "Enhancing Activity and Stability of Cobalt Oxide Electrocatalysts for the Oxygen Evolution Reaction via Transition Metal Doping For Increased Enhancing Activity and Stability of Cobalt Oxide Electrocatalysts for the Oxygen Evolution Reaction via Transition Metal Doping," ECS., Vol. 163, No. 3, **2016**.

[23] C. Kuo *et al.*, "Understanding the Role of Gold Nanoparticles in Enhancing the Catalytic Activity of Manganese Oxides in Water Oxidation Reactions ** Angewandte," GDCH., Vol. 54, No. 8, pp. 1–7, **2014**.

[24] V. A. Online, " Porpus β-MnO_2 nanoplates derived from $MnCO_3$ nanoplates as highly efficient electrocatalysts toward oxygen evolution reaction †," RSC Advances., Vol. 2, No. 6, pp. 26535–26539, **2016**.

[25] Y. Gorlin and T. F. Jaramillo, "A Bifunctional Nonprecious Metal Catalyst for Oxygen Reduction and Water Oxidation," ACS Publications., Vol. 132, No. 39, pp. 13612–13614, **2010**.

[26] X. Liu, S. Cui, Z. Sun, Y. Ren, X. Zhang, and P. Du, "Self-Supported Copper Oxide Electrocatalyst for Water Oxidation at Low Overpotential and Confi rmation of Its Robustness by Cu K - Edge X - ray Absorption Spectroscopy," ACS Publications., Vol. 120, No. 2, **2016**.

[27] J. A. Bau *et al.*, "Nickel/Iron Oxide Nanocrystals with a Nonequilibrium Phase: Controlling Size, Shape, and Composition," ACS Publications, Vol 26, No. 16, **2014**.

[28] W. Xia, N. Li, Q. Li, K. Ye, and C. Xu, "Au-$NiCo_2O_s$ supported on three-dimensional hierarchical porous graphene-like material for highly effective oxygen evolution reaction," *Nat. Publ. Gr.*, Vol. 6, pp. 1–9, **2016**.

[29] Y. Lee, A. Grimaud, and Y. Shao-horn, "Influence of Oxygen Evolution during Water Oxidation on the Surface of Perovskite Oxide Catalysts," ACS Publications, Vol. 3, No. 22, pp. 3264-3270, **2012**.

[30] M. S. Burke, M. G. Kast, L. Trotochaud, A. M. Smith, and S. W. Boettcher, "Cobalt − Iron (Oxy) hydroxide Oxygen Evolution Electrocatalysts : The Role of Structure and Composition on Activity , Stability , and Mechanism," ACS Publications., Vol. 137, No. 10, pp. 3638-3648, **2015**.

[31] X. Liu *et al.*, "Hierarchical $NiCo_2O_4$ @ $NiCo_2O_4$ Core / Shell Nano flake Arrays as High- Performance Supercapacitor Materials," ACS Publications., Vol. 5, No. 7, pp. 8790-8795, **2013**.

[32] A. Sayeed, T. Herd, and A. P. O. Mullane, "Direct electrochemical formation of nanostructured amorphous $Co(OH)_2$ on gold evolution reaction †," RSC., Vol. 4, pp. 991–999, **2016**.

[33] D. Zhang, J. Li, J. Luo, P. Xu, and L. Wei, "Ni_3S_2 nanowires grown on nickel foam as an efficient bifunctional electrocatalyst for water splitting with greatly practical prospects." NanoTechnology., Vol 29. No. 24, **2018**.

[34] Y. Liu *et al.*, "Low Overpotential in Vacancy-Rich Ultrathin $CoSe_2$ Nanosheets for Water Oxidation," ACS Publications., Vol. 136, No. 44, **2014**.

[35] L. A. Stern, L. Feng, F. Song, and X. Hu, "Ni_2P as a Janus catalyst for water splitting: The oxygen evolution activity of Ni_2P nanoparticles," *Energy Environ. Sci.*, Vol. 8, No. 8, pp. 2347–2351, **2015**.

[36] K. Oda and T. Yoshio, "Preparation of Co-N films by rf-sputtering," Springer Link., Vol. 22, pp. 2729–2730, **1987**.

[37] L. Wu *et al.*, "Stable Cobalt Nanoparticles and Their Monolayer Array as an," ACS Publications., Vol. 137, No. 22, pp. 7071-7074, **2015**.

[38] Y. Yang, H. Fei, G. Ruan, C. Xiang, and J. M. Tour, " Efficient Electrocatalytic Oxygen Evolution on Amorphous Nickel À Cobalt Binary Oxide," ACS Publications., Vol. 8, No. 9, pp. 9518–9523, **2014**.

[39] A. Eftekhari, "From pseudocapacitive redox to intermediary adsorption in oxygen evolution reaction," *Mater. Today Chem.*, vol. 4, pp. 117–132, **2017**.

[40] A. Eftekhari and F. Molaei, "Carbon nanotube-assisted electrodeposition . Part II : Superior pseudo-capacitive behavior of manganese oxide film electrodeposited at high current densities," *J. Power Sources*, Vol. 274, pp. 1315–1321, **2015**.

[41] A. Y. Faid, A. O. Barnett, F. Seland, and S. Sunde, "Optimized Nickel-Cobalt and

Nickel-Iron Oxide Catalysts for the Hydrogen Evolution Reaction in Alkaline Water Electrolysis," *J. Electrochem. Soc.*, Vol. 166, No. 8, pp. F519–F533, **2019**.

[42] M. Gong and H. Dai, "A mini review of NiFe-based materials as highly active oxygen evolution reaction electrocatalysts," *Nano Res.*, Vol. 8, No. 1, pp. 23–39, **2014**.

[43] K. Fominykh *et al.*, "Ultrasmall dispersible crystalline nickel oxide nanoparticles as high-performance catalysts for electrochemical water splitting," *Adv. Funct. Mater.*, Vol. 24, No. 21, pp. 3123–3129, **2014**.

[44] K. Fominykh *et al.*, "Iron-doped nickel oxide nanocrystals as highly efficient electrocatalysts for alkaline water splitting," *ACS Nano*, Vol. 9, No. 5, pp. 5180–5188, **2015**.

[45] X. Liu, W. Liu, M. Ko, M. Park, M. G. Kim, and P. Oh, "Metal (Ni , Co) -Metal Oxides / Graphene Nanocomposites as Multifunctional Electrocatalysts," Advanced Functional Materials., Vol. 25, No. 36, pp. 5799–5808, **2015**.

[46] X. Zhang, H. Xu, X. Li, Y. Li, T. Yang, and Y. Liang, "Facile Synthesis of Nickel-Iron/Nanocarbon Hybrids as Advanced Electrocatalysts for Efficient Water Splitting," *ACS Catal.*, Vol. 6, No. 2, pp. 580–588, **2016**.

[47] L. Trotochaud, S. L. Young, J. K. Ranney, and S. W. Boettcher, "Nickel-Iron oxyhydroxide oxygen-evolution electrocatalysts: The role of intentional and incidental iron incorporation," *J. Am. Chem. Soc.*, Vol. 136, No. 18, pp. 6744–6753, **2014**.

[48] R. Xiang *et al.*, "Hierarchical coral-like $FeNi(OH)_x$ /Ni via mild corrosion of nickel as an integrated electrode for efficient overall water splitting," *Cuihua Xuebao/Chinese J. Catal.*, Vol. 39, No. 11, pp. 1736–1745, **2018**.

[49] G. Wu *et al.*, "Hierarchical Fe-doped NiO_x nanotubes assembled from ultrathin nanosheets containing trivalent nickel for oxygen evolution reaction," *Nano Energy*, vol. 38, pp. 167–174, **2017**.

[50] R. Zhang *et al.*, "Enhanced electrocatalytic activity for water splitting on NiO/Ni/carbon fiber paper," *Materials (Basel).*, vol. 10, No. 1, pp. 1–8, **2017**.

[51] M. W. Louie and A. T. Bell, "An investigation of thin-film Ni-Fe oxide catalysts for the electrochemical evolution of oxygen," *J. Am. Chem. Soc.*, Vol. 135, No. 33, pp. 12329–12337, **2013**.

[52] C. R. P. Patel *et al.*, "Enhanced hydrogen generation by water electrolysis employing carbon nano-structure composites," *Int. J. Hydrogen Energy*, Vol. 43, No. 6, pp. 3180–3189, **2018**.

[53] M. Gong *et al.*, "Nanoscale nickel oxide/nickel heterostructures for active hydrogen evolution electrocatalysis," *Nat. Commun.*, Vol. 5, pp. 1–6, **2014**.

[54] M. Görlin *et al.*, “Oxygen evolution reaction dynamics, faradaic charge efficiency, and the active metal redox states of Ni-Fe oxide water splitting electrocatalysts,” *J. Am. Ckihem. Soc.*, Vol. 138, No. 17, pp. 5603–5614, **2016**.

[55] Y. Xu *et al.*, “Supercritical CO_2 -Assisted synthesis of $NiFe_2O_4$ / vertically-aligned carbon nanotube arrays hybrid as a bifunctional electrocatalyst for effi cient overall water splitting,” *Carbon N. Y.*, Vol. 145, pp. 201–208, **2019**.

[56] A. Qayoom Mugheri *et al.*, “Co_3O_4 / NiO bifunctional electrocatalyst for water splitting,” *Electrochim. Acta*, vol. 306, pp. 9–17, **2019**.

[57] S. Wu *et al.*, “Fluorine-doped nickel cobalt oxide spinel as efficiently bifunctional catalyst for overall water splitting,” *Electrochim. Acta*, Vol. 299, pp. 231–244, **2019**.

[58] H. Yu *et al.*, “Prompt Electrodeposition of Ni Nanodots on Ni Foam to Construct a High-Performance Water-Splitting Electrode: Efficient, Scalable, and Recyclable,” *Nano-Micro Lett.*, vol. 11, no. 1, 2019.

[59] A. Mondal, A. Paul, D. N. Srivastava, and A. B. Panda, “NiO hollow microspheres as efficient bifunctional electrocatalysts for Overall Water-Splitting,” *Int. J. Hydrogen Energy*, Vol. 43, No. 47, pp. 21665–21674, **2018**.

[60] L. Peng *et al.*, “Rationally design of monometallic NiO-Ni_3S_2 /NF heteronanosheets as bifunctional electrocatalysts for overall water splitting,” *J. Catal.*, Vol. 369, pp. 345–351, **2019**.

[61] F. Song *et al.*, “An Unconventional Iron Nickel Catalyst for the Oxygen Evolution Reaction,” *ACS Cent. Sci.*, Vol. 5, No. 3, pp. 558–568, **2019**.

[62] E. N. Kaufmann, "*Characterizarion of materials*," Wiley., 1st ed. **2003**.

[63] Tolen, Metin, "*Microscopy and Scattering / Diffraction Microscopy with soft matter surfaces and organic thin films*." springer., 1st ed, **1999**.

[64] P. Solanki, A. Kumar, A. Garg, P. Sharma, and S. Singh, “Designing & Development of Spherical Agglomerates of Ibuprofen-Paracetamol Blend for Improved Tableting and Dissolution,” *Int. J. Ther. Appl.*, Vol. 8, pp. 8–13, **2012**.

[65] A. Alexander, “The nature and origin of ancient oxygen isotopic heterogeneities in Mars ’ crust,” CU Scholar., **2018**.

[66] S. Swapp, “Scanning electron microscopy,” *Geochemical intrumentation Anal. , Univ. wyoming*, **2009**.

[67] M. Felty, “Adsorption of Propane on the Magnesium Oxide (100) Surface and Synthesis of Anodized Aluminum Oxide,” University of Tennessee., **2008**.

[68] S. P. Charu Dwivedi, “Electrospun Nanofibrous scaffolds as a potential carrier of antimicrobial therapeutics for diabetic wound healing and tissue reengineering,”

Nano microscale drug deivery Syst, Chapter:9, Elsevier Inc., pp.147-164, **2017**.

[69] K. Alawam, "protreomics in Biomedicine and Pharmacology," *Adv. protien Chem. Struct. Biol.,* **2014**.

[70] K. Dipesh, S. Bhaskar, B. Kuldeep, and K. John, "Bio-oil and biodiesel as biofuesl derived from microalgal oil and their characterization by using instrumental techniques," *Algae Environ. Sustain.,* ppt. 87-96, **2015**.

[71] N. Bchellaoui, Z. Hayat, M. Mami, R. Dorbez-Sridi, and A. I. El Abed, "Microfluidic-assisted Formation of Highly Monodisperse and Mesoporous Silica Soft Microcapsules," *Sci. Rep.*, Vol. 7, No. 1, pp. 1–10, **2017**.

[72] I.Chemicals, "IntertekWhitepaper_Surface_Area_and_Porosity_Chemicals170613," Intertek., **2013**.

[73] "Cyclic voltametry," *LibreText,* **2019**.

[74] V. Climent and J. M. Feliu, "Cyclic Voltammetry," *Encycl. Interfacial Chem.*, Vol. 2, No. 2, pp. 48–74, **2018**.

[75] N. Elgrishi, K. J. Rountree, B. D. McCarthy, E. S. Rountree, T. T. Eisenhart, and J. L. Dempsey, "A Practical Beginner's Guide to Cyclic Voltammetry," *J. Chem. Educ.*, Vol. 95, No. 2, pp. 197–206, **2018**.

[76] J. Qi *et al.*, "Porous Nickel–Iron Oxide as a Highly Efficient Electrocatalyst for Oxygen Evolution Reaction," *Adv. Sci.*, Vol. 2, No. 10, pp. 1–8, **2015**.